united nations
lucational, scientific
and cultural
organization

international atomic
energy agency

the
abdus salam
international centre for theoretical physics

SMR 1161/4

AUTUMN COLLEGE ON PLASMA PHYSICS

25 October - 19 November 1999

Self-Organized Vortical Motions in Magnetized Plasmas

Mitsuo Kono

Chuo University
Tokyo, Japan

Contents

Chapter 1

Introduction

Self-organization is one of the most important key notions in various fields such as physical sciences, life sciences and even in social sciences. Formation of self-organized structures in magnetized plasmas has been a topic since studies of such coherent structures may give a scenario common to self-organization in complex systems as well as transport phenomena in plasmas. In fact coherent structures have been recently observed in laboratories [1-5] and are subject to theoretical analysis for understanding underlying physics.

Two dimensional turbulent fluids and plasmas have been widely recognized to self-organize into large scale coherent structures [6-21]. One of such examples is given in Fig.1.1 which shows that the collisional drift wave instability evolves into a dipole vortex [22]. This kind of self-organization has been observed in numerous systems like geostrophic fluids, planetary atmospheric fluids, and guiding center plasmas. A huge number of works have been done on relaxation of two dimensional turbulence to organized motions and it is believed that a fair understanding of self-organization in two dimension has been achieved: the fundamental phenomena can be explained by the scenario of either selective decay hypothesis [6-10] or maximal entropy principle [11-20]. Therefore three dimensional turbulence is often emphasized to be studied instead. However there are still important problems left unsolved in two dimensional turbulence. In a course of time evolution of self-organization the number of vortices decreases. According to experiments and numerical simulations the number of vortices decays algebraically, which is not properly understood. The emergence of self-organized motions has been observed experimentally in a magnetically confined pure electron columns by K. S. Fine, A. C. Case, W. G. Flynn and C. F. Driscoll [2] and numerically in decaying and force-driven drift wave turbulence by N. Kurkhakin, S. A. Orszag and V. Yakhot [25] and T.Watanabe et al [26]. Both observations are commonly concerning long-lived ordered motions (crystallization) of well defined vortices, suggesting that the relaxation to the ordered states may be described by introducing point vortices [27,28] with which partial differential equations designed to describe vortical motions are converted to a set of ordinary differential equations. In fact dynamics based on point vortices is shown to recover almost the same dynamical behaviors obtained by solving

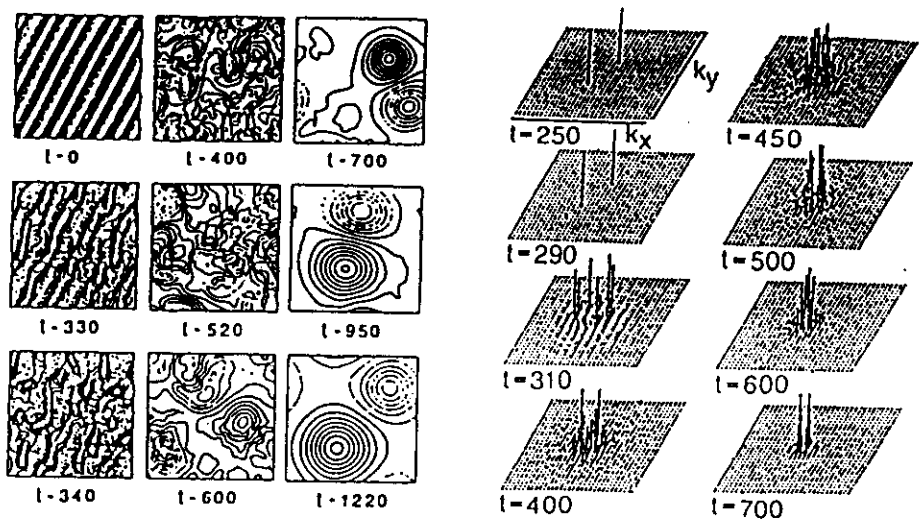

Figure 1.1: (a) The time evolution of the spatial structure of the potential obtained by solving eq.(18) in Sec. 2 for $\kappa = \nu = 0.3$ and $\delta = 0.1$. The contours of the potential are normalized by the maximum amplitude at each time step. The solid and dotted contours represent the positive and negative parts of the potential, respectively. (b) The time evolution of the spectrum of the potential for the same parameters as those in (a). The amplitudes are normalized by the maximum value at each time step.

the partial differential equation for the collisional drift wave instability [27-35]. Another example of the emergence of self-organization is spiral structures which have been observed in both ECR plasmas [4] and gun-produced plasmas [5]. The common feature of the observed spirals is a two-arm structure. Although there is an effort [36] to understand the physics behind the vortex crystallization by modifying the maximal entropy principle, these findings such as vortex crystallization and spirals need new approaches which seem beyond the scope of the existing scenarios.

In the next chapter the emergence of organization through turbulent states in the course of time evolution of the collisional drift wave instability is discussed and the scenarios of self-organization are reviewed and a scaling theory is formulated to explain the decay of the number of vortices in chapter 3. In chapter 4 based on the point vortex description dynamical properties of vortices such as collision processes, the vortex collapse and diffusion process is studied dynamically and statistically. In chapter 5 the dynamics of the drift wave vortices in cylindrical plasmas is studied and in chapter 6 the collective behaviors of vortices are examined. In chapter 7 spiral structures in ECR plasmas will be discussed associated with the collisional drift wave instability.

References

[1] M.V.Nezlin and E.N.Snezhkin, *Rossby Vortices, Spiral Structures, Solitons*,(Springer-Verlag, Berlin,1993)

[2] K.S.Fine, A.C.Case, W.G.Flynn and C.F.Driscoll, Phys. Rev. Lett. **75**, 3277 (1995)

[3] Y.Amagishi, Y.Yoshikawa and J.Ohara, J.Phys.Soc.Jpn **60**, 2496 (1992)

[4] M.Y.Tanaka, T.Sakamoto, H.Imaizumi, K.Taniguchi and Y.Kawai, Proc. 1996 Int. Conf. on Plasma Physics(Nagoya, Japan) Vol.2, 1650 (1997)

[5] T.Ikehata, H.Tanaka, N.Y.Sato and H.Mase, Phys. Rev. Lett. **81**, 1853 (1998)

[6] R.H.Kraichnan, Phys. Fluids **10**, 1417(1967) [7] C.E.Seyler, Y.Salu, D.Montgomery and G.Knorr, Phys. Fluids **18**, 803 (1975)

[8] R.H.Kraichnan and D. Montgomery, *Repts. Progress in Physics* **43**, 547 (1980)

[9] A.C.Ting, W.H.Matthaeus and D.Montgomery, Phys. Fluids **29**, 3261 (1986)

[10] W.H.Matthaeus, W.T.Stribling, D.Martinez, S.Oughton and D.Montgomery, Phys. Rev. Letters **66**, 2731(1991)

[11] L.Onsager, Nuovo Cimento Suppl. **6**, 279 (1949)

[12] D.Montgomery, Phys. Letters **39A**, 7 (1972)

[13] J.B.Taylor, Phys. Letters **40A**, 1 (1972)

[14] G. Joyce and D.Montgomery, J. Plasma Phys. **10**, 107 (1973)

[15] D. Montgomery and G. Joyce, Phys. Fluids **17**, 1139 (1974)

[16] A.C.Ting, H.Chen and Y.C.Lee, Physica **D26**, 37 (1987)

[17] J.C.McWilliams, J. Fluid Mech. **219**, 316 (1990)

[18] D. Montgomery, Phys. Rev. **A44**, 6437 (1991)

[19] R.A.Smith, Phys. Rev. **A43**, 1126 (1991)

[20] G.L.Eyink and H.Spohn, J. Stat. Phys. **70**, 833 (1993)

[21] W. Horton, D. I. Choi and W. M. Tang: Phys. Fluids **24**, 1077 (1981)

[22] M.Kono and E.Miyashita, Phys. Fluids **31**, 326 (1988)

[23] K. S. Fine, A. C. Case, W. G. Flynn and C. F. Driscoll, Phys. Rev. Letters **75**, 3277 (1995)

[24] C.E.Seyler, J. Plasma Phys. **56**, 533 (1996)

[25] N. Kukharkin, S. A. Orszag and V. Yakhot, Phys Rev. Lett. **75**, 2468 (1995)

[26] T.Watanabe, H.Fujisaka and T.Iwayama, Phys. Rev. **E55**, 5575 (1997)

[27] H. Aref, Phys. Fluids **22**, 393 (1979)

[28] E. A. Novikov and Yu B. Sedov, Sov. Phys. JETP **48**, 440 (1978)

[29] M. Kono and W. Horton, Phys. Fluids **B3**, 3255 (1991)

[30] D. Hobson, Phys. Fluids **A3**, 3027 (1991)

[31] H. Shibahara and M. Kono, Phys. Fluids **B4**, 2992 (1992)

[32] H. Shibahara and M. Kono, Chaos, Soliton & Fractals **2**, 597 (1992)

[33] K. Yabuki, K. Ueno and M. Kono, Phys. Fluids **B5**, 2853 (1993)

[34] K. Yabuki and M. Kono, Phys. Fluids **B5**, 3103 (1993)

[35] M. Kono, H. Shibahara and K. Yabuki, AIP Conf. Proc. # 284, 539 (1994)

[36] D.Z.Jin and D.H.E.Dubin, *Phys. Rev. Letters* **80**, 4434 (1998)

Chapter 2

Collisional drift wave instability and formation of dipole vortex

Nonlinear dynamics of drift waves has been subject to intensive studies since these waves are regarded as responsible for anomalous transport in plasmas. Hasegawa and Mima [1] derived a model equation to explain the high level of density fluctuations and the broad frequency spectrum observed in a tokamak [2]. Since then, many properties of drift wave turbulence have been revealed: the spectrum evolution is characterized by an inverse cascade [3], the wavenumber spectrum obeys the Kolgomolov-Kraichnan law k^{-3} [4,5], the broad frequency spectrum is demonstrated in several ways based on such a soliton gas model [6,7] and a truncated mode-coupling model exhibiting chaos [8,9], the saturation in an unstable system is initiated by the $\mathbf{E} \times \mathbf{B}$ drift [10], etc.

On the other hand, the Hasegawa-Mima equation is known to have vortex-pair solutions [11]. These dipole vortices have been shown to be fairly stable against collisions and perturbations [12,13], although in the strict sense they are not as stable as solitons. Thus the Hasegawa-Mima equation is anticipated to link strong turbulence to self-organized motions. Similar phenomena of self-organization have been demonstrated in two-dimensional hydrodynamic turbulence [14,15] and in magnetohydrodynamic turbulence [16-17].

In this chapter, we study the formation of a coherent structure vir turbulence in the course of nonlinear development of the collisional drift wave instability. In Sec.2.1, we extend the Hasegawa-Mima equation so as to be applicable to an unstable systems. Numerical simulations based on the model equation are performed in Sec.2.2 to establish a scenario for the instability evolution: linear growth is followed by a parametric instability that excites small scale vortices. These vortices then fuse into larger vortices as a results of an inverse cascade, leading finally to a large single dipole vortex. The last section 2.3 is devoted to discussion.

2.1 Derivation of the model equation

The dynamical equation describing the evolution of the electrostatic potential $\psi(\mathbf{r},t)$ is obtained from a two-fluid model:

$$\frac{\partial n_e}{\partial t} + \nabla \cdot (n_e \mathbf{v_e}) = 0, \tag{2.1}$$

$$n_e m(\frac{\partial}{\partial t} + \mathbf{v_e} \cdot \nabla)\mathbf{v_e} = -\nabla p_e - e n_e(\mathbf{E} + \frac{\mathbf{v_e}}{c} \times \mathbf{B}) + \mathbf{R}, \tag{2.2}$$

$$\frac{\partial n_i}{\partial t} + \nabla \cdot (n_i \mathbf{v_i}) = 0, \tag{2.3}$$

$$n_i M(\frac{\partial}{\partial t} + \mathbf{v_i} \cdot \nabla)\mathbf{v_i} = -\nabla p_i + e n_i(\mathbf{E} + \frac{\mathbf{v_i}}{c} \times \mathbf{B}) + \mathbf{R} - \nabla \cdot \mathbf{\Pi}, \tag{2.4}$$

$$\tag{2.5}$$

with the quasineutrality condition

$$n_e \simeq n_i = n.$$

The magnetic field is homogeneous and in the z direction,while the background density gradient is in the x direction specified by $\eta = -(d/dx)\ln n_0 = const.$ The frictional force $\mathbf{R}$ and the stress tensor $\mathbf{\Pi}$ are given by Braginskii [18]. The electron viscosity is neglected because of its smallness. In the following, we consider the case where both electron and ion temperature are homogeneous and electrostatic waves propagate almost perpendicular to the magnetic field ($k_\perp >> k_\parallel$). Then the motions perpendicular to the magnetic field are

$$\mathbf{v}_e = \mathbf{v}_E + \mathbf{v}_{De}, \tag{2.6}$$

$$\mathbf{v}_i = \mathbf{v}_E + \mathbf{v}_{Di} + \mathbf{v}_p, \tag{2.7}$$

where $\mathbf{v}_E$, $\mathbf{v}_D$ and $\mathbf{v}_p$ are the $\mathbf{E}\times\mathbf{B}$ drift, diamagnetic drift, and polarization drift, respectively. These are given by

$$\mathbf{v}_E = -(\nabla\psi \times \mathbf{z})/B, \tag{2.8}$$

$$\mathbf{v}_D = -sgn(e_\alpha)\frac{v_{T\alpha}^2}{\Omega_\alpha}(\nabla_\perp \ln n_\alpha \times \mathbf{z}),\ (\alpha = e,i), \tag{2.9}$$

$$\mathbf{v}_p = \frac{1}{\Omega_i}[(\frac{\partial}{\partial t} + \mathbf{u}_i \cdot \nabla_\perp)\mathbf{u}_i + \frac{1}{n_i M}\nabla_\perp \cdot \mathbf{\Pi}] \times \mathbf{z}, \tag{2.10}$$

where

$$\mathbf{u}_i = \mathbf{v}_E + \mathbf{v}_{Di}.$$

Substituting eqs.(2.6) and (2.7) into the continuity equations, we obtain

$$\frac{\partial}{\partial t}n_e + (\mathbf{v_e} \cdot \nabla_\perp)n_e + \nabla_\parallel(n_e v_{e\parallel}) = 0, \tag{2.11}$$

$$\frac{\partial}{\partial t}n_i + (\mathbf{v_i} \cdot \nabla_\perp)n_i + \nabla_\perp \cdot (n_i \mathbf{v}_p) + \nabla_\parallel(n_i v_{i\parallel}) = 0. \tag{2.12}$$

For the ion motion parallel to B, we may neglect the viscosity and have

$$\frac{\partial}{\partial t}\mathbf{v}_{i\parallel} + (\mathbf{v}_i \cdot \nabla)\mathbf{v}_{i\parallel} = -\frac{1}{n_i M}\nabla_\parallel p_i - \frac{e}{M}\nabla_\parallel \psi. \tag{2.13}$$

Since the electron inertia is so small, the electron parallel velocity may be approximated as

$$v_{e\parallel} \simeq D_\parallel \nabla_\parallel (\frac{e\psi}{T_e} - \ln n_e), \tag{2.14}$$

where $D_\parallel = T_e/m\nu_{ei}$. Then eq.(2.11) is linearized with respect to the fluctuation to give the electron density fluctuation in terms of the potential after an iteration. This is based on the fact that the deviation of the electron density from the Boltzman distribution may be assumed small:

$$\tilde{n}_e \simeq n_{e0}[1 - \frac{1}{k_\parallel^2 D_\parallel}(\frac{\partial}{\partial t} + v_{De}\frac{\partial}{\partial y})]\frac{e\psi}{T_e}. \tag{2.15}$$

Invoking the quasineutrality condition and retaining the terms up to ε [$\varepsilon = \rho/L_n$, $\rho = C_s/\Omega_i$, $C_s = (T/M)^{1/2}$, $\Omega_i = eB/Mc$, and $L^{-1} = (\partial/\partial x)\ln n_0$], we obtain the model equations describing the nonlinear evolution of the collisional drift wave instability:

$$[(1 - \kappa\frac{\partial}{\partial t})(\frac{\partial}{\partial t} + \frac{\partial}{\partial y}) - (\frac{\partial}{\partial t} + \frac{\partial}{\partial y} - \nu\delta\nabla^2)\nabla^2]\psi + \frac{\partial}{\partial z}v_z = (\mathbf{z} \times \nabla_\perp\psi)\cdot\nabla_\perp\nabla_\perp^2\psi, \tag{2.16}$$

$$\frac{\partial}{\partial t}v_z + \frac{\partial}{\partial z}\psi = -(\mathbf{z} \times \nabla_\perp\psi)\cdot\nabla_\perp v_z, \tag{2.17}$$

where the following replacements are used:

$$\kappa = \frac{C_s}{D_\perp k_\parallel^2 L_n},\ \nu = \frac{3}{10}\frac{L_n}{C_s\tau_i},\ \delta = \frac{T_i}{T_e},$$

with the normalizations

$$x \to \rho x,\ z \to L_n z,\ t \to \frac{L_n}{C_s}t,\ \frac{e\psi}{T_e} \to \psi,\ \frac{v_{i\parallel}}{C_s} \to v_z.$$

When collisions and viscosity are neglected, a set of equations is shown by Meiss and Horton [20] to have dipole solutions as stationary solutions. This may suggest that the evolution of the collisional drift wave instability governed by eqs.(2.16) and (2.17) eventually leads to the formation of dipole vortices. However, three-dimensional dynamics are seemingly quite complicated. In the following, we restrict our attention to evolution in a two-dimensional system for which the ion motion in the z direction is neglected in eqs.(2.16) and (2.17). This reduction of the dimensionality physically corresponds to the case where ion acoustic waves are decoupled from the drift waves, and is verified when $k_\perp >> k_\parallel$. Furthermore, invoking the result that $\partial/\partial t + \partial/\partial y \simeq 0$ for waves with a long wavelength, the collisional term responsible for the instability, $\kappa\partial/\partial t$ is replaced by $-\kappa\partial/\partial y$. Thus eqs.(2.16) is decoupled from (2.17) to give a single nonlinear equation:

$$\frac{\partial}{\partial t}(1 - \nabla_\perp^2 + \kappa\frac{\partial}{\partial y})\psi + [(\frac{\partial}{\partial y} + \kappa\frac{\partial^2}{\partial y^2}) - \delta(\frac{\partial}{\partial y} - \nu\nabla^2)\nabla^2]\psi = [(\mathbf{z} \times \nabla_\perp\psi)\cdot\nabla_\perp]\nabla_\perp^2\psi, \tag{2.18}$$

which is the Hasegawa-Mima equation extended to describe drift waves in an unstable system.

The dispersion relation of a linear wave is obtained from eq.(2.18) for the real frequency as

$$\omega(\mathrm{k}) = \frac{k_y}{(1+k^2)^2 + \kappa^2 k_y^2}[(1+k^2)(1+\delta k^2) + \kappa(\kappa k_y^2 - \nu\delta k^4)], \tag{2.19}$$

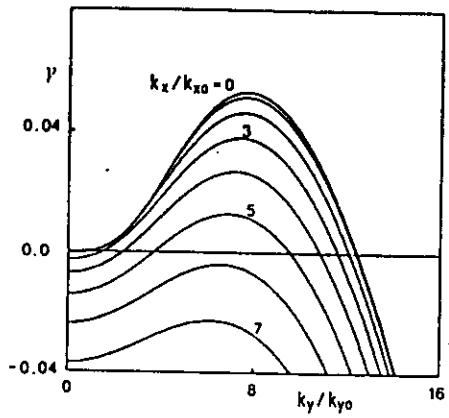

Figure 2.1: The growth rates against k_y for fixed $k_x/k_0 = 0 - 7$ in the case of $\kappa = \nu = 0.3$ and $\delta = 0.1$.

and for the instability growth rate as

$$\gamma(\mathrm{k}) = \frac{k^2}{(1+k^2)^2 + \kappa^2 k_y^2}[\kappa(1-\delta)k_y^2 - \nu\delta k^2(1+k^2)], \tag{2.20}$$

which are compared with those used by Terry and Horton [8] with the out-of-phase component for $k_\parallel v_{Te} < \nu_{ei}$ [20]. In Fig.2.1 the growth rate $\gamma(\mathrm{k})$ is depicted against k_y for various values of k_x at $\kappa = \nu = 0.3$ and $\delta = 0.1$ The spectral structure of the growth rate is characterized by the finite bandwidth for the instability, which itself manifests a possibility of forming a coherent structure.

A stationary solution of Eq.(2.18), with $\kappa = \nu = \delta = 0$ referred to as a dipole vortex, is given by

$$\psi(r,\theta) = \begin{cases} \dfrac{acK_1(\beta r/a)}{K_1(\beta)}\cos\theta, & for\ r > a \\ ac[(1+\dfrac{\beta^2}{\gamma^2})\dfrac{r}{a} - \dfrac{\beta^2 J_1(\gamma r/a)}{\gamma^2 J_1(\gamma)}]\cos\theta, & for\ r < a, \end{cases} \tag{2.21}$$

where $r^2 = x^2 + (y - ct)^2$, $\cos\theta = x/r$, $\beta = a(1 - 1/c)^{1/2}$, and a and c are parameters characterizing the size and speed of the dipole vortex, respectively. The J_1 and K_1 are the Bessel function of the first kind and the modified Bessel function of the second kind. Here γ is determined through the following equation

$$\frac{K_2(\beta)}{\beta K_1(\beta)} = -\frac{J_2(\gamma)}{\gamma J_1(\gamma)}, \tag{2.22}$$

which gives an infinite number of γ for a fixed β. The dipole vortex solution is given for the smallest value of γ. For larger values of γ the number of nodes increases, giving excited states shown in Fig.2.2(a). Although the stationary solution with the smallest γ is known stable, the excited states are unstable and throw the dress off to become to the dipole vortex as they propagate shown if Fig.2.2(b).

2.2 The simulations

In solving eq.(2.18), we used the algorithm developed by Gourlay and Moris [21]. The number of mesh points is 128 × 128 and the periodic boundary conditions are imposed. The stability of the numerical

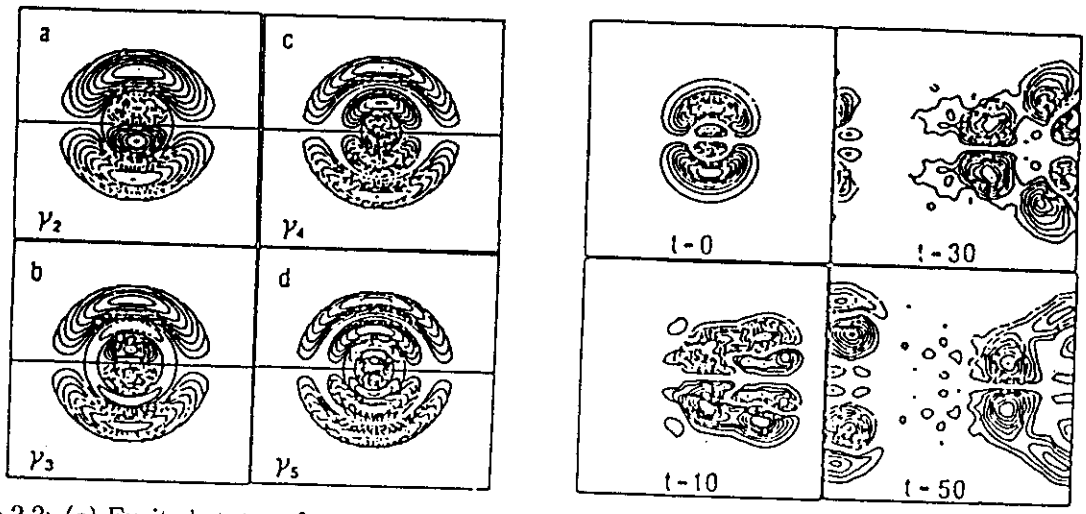

Figure 2.2: (a) Excited states of stationary solutions and (b) the time evolution of the excited state with γ_2.

scheme is ensured by monitoring changes in conserved quantities of eq.(2.18) without the collision and viscosity, that is, the Hasegawa-Mima equation. For eq.(2.18) we launched many waves at the initial moment and confirmed that the observed growth rate spectra agree well with the theoretical linear growth rate spectra. Simulations with a higher resolution (256 × 256 grids) performed for several parameters confirmed the results in the 128 × 128 simulations. This is because, as a result of the viscosity in eq.(2.18), short waves are heavily damped and play no role in the physics.

The initial condition is chosen as

$$\psi(x, y, t = 0) = \psi_0 \sin(k_x x + k_y y),$$

$$(k_x, k_y) = (2k_0, 4k_0), \quad (k_0 = \pi/16),$$

with the amplitude $\psi_0 = 0.001$ for $\kappa = \nu = 0.3$ and $\delta = 0.1$. The course of development is shown in Fig.1.1, in which the contour of the potential and the spectrum are depicted, respectively. The maximum amplitudes of the potential and the spectrum at each time step are used for the normalization. The wave grows at the linear growth rate $\gamma \simeq 0.023$, followed by an excitation of higher harmonics. Around $t = 300$, when the amplitude of the initially launched waves exceeds a certain value of about $\psi_0 e^{\gamma t} \simeq 0.99$, energy transfer to many modes occurs abruptly (from $t = 290$ to $t = 310$ in Fig.1.1(b)), leading to the breakup of the wave into a train of small vortices. This secondary instability is identified with the parametric instability as follows. By Fourier transforming eq.(2.18), we obtain

$$(\frac{\partial}{\partial t} + i\omega(\mathrm{k}) - \gamma(\mathrm{k}))\psi(\mathrm{k}) = \sum_{\mathrm{k}'+\mathrm{k}''=\mathrm{k}} \Lambda_k(\mathrm{k}', \mathrm{k}'')\psi(\mathrm{k}')\psi(\mathrm{k}''), \tag{2.23}$$

where $\omega(\mathrm{k})$ and $\gamma(\mathrm{k})$ are given by eqs.(2.19) and (2.20), respectively, and

$$\Lambda_k(\mathrm{k}', \mathrm{k}'') = \frac{1}{2}\frac{(\mathrm{k}' \times \mathrm{k}'') \cdot \mathrm{z}}{1 + k^2 + i\kappa k_y}(k''^2 - k'^2). \tag{2.24}$$

Taking the initially launched waves $\mathbf{k} = (2k_0, 4k_0)$ and $(-2k_0, -4k_0)$ as a pump since they already have grown up to the finite amplitude, the conventional analysis for the parametric interaction yields the growth rate Γ and the frequency shift Ω as

$$\Gamma = \frac{1}{2}[\gamma(\mathbf{k}_1) + \gamma(\mathbf{k} - \mathbf{k}_1)] \pm \frac{1}{\sqrt{2}}[(A^2 + B^2)^{1/2} + A]^{1/2}, \tag{2.25}$$

$$\Omega = \pm\frac{1}{\sqrt{2}}[(A^2 + B^2)^{1/2} - A]^{1/2}, \tag{2.26}$$

where

$$A = \frac{1}{4}\{[\gamma(\mathbf{k}_1) - \gamma(\mathbf{k} - \mathbf{k}_1)]^2 - \Delta^2\} + |\psi_0|^2 \Re G, \tag{2.27}$$

$$B = \frac{1}{2}\Delta[\gamma(\mathbf{k}_1) - \gamma(\mathbf{k} - \mathbf{k}_1)] + |\psi_0|^2 \Im G, \tag{2.28}$$

$$\Delta = \omega(\mathbf{k}) - \omega(\mathbf{k}') - \omega(\mathbf{k} - \mathbf{k}_1), \tag{2.29}$$

$$G = \frac{[(\mathbf{k}' \times \mathbf{k}'') \cdot \mathbf{z}]^2 (k^2 - k_1^2)}{(1 + k^2 + i\kappa k_y)[1 + (\mathbf{k} - \mathbf{k}_1)^2 + i\kappa(\mathbf{k} - \mathbf{k}_1)_y]}. \tag{2.30}$$

Since $\gamma(\mathbf{k})$ is of the order of κ, the threshold for the instability is roughly estimated by

$$|\psi_0|^2_{th} \simeq \frac{\Delta^2}{e\Re G}, \tag{2.31}$$

which is meaningful only when $G > 0$, that is,

$$min[k_1^2, (\mathbf{k} - \mathbf{k}_1)^2] < k^2 < max[k_1^2, (\mathbf{k} - \mathbf{k}_1)^2]. \tag{2.32}$$

A set of the wavenumber $\mathbf{k}_1$ satisfying the relation (2.32) for the $\mathbf{k} = (2k_0, 4k_0)$, is shown by solid points in Fig.2.3, which, together with the points symmetric with respect to the origin for the pump of $(-2k_0, -4k_0)$, reproduces the observed structure of the spectrum. The small vortices excited as a results of the parametric instability then interact to fuse into larger ones. The inverse cascade of the wave energy on the spectrum clearly observed in Fig.1.1 is responsible for the fusion of vortices. Finally, one large dipole vortex is formed and propagates in a rotating manner. In Fig.2.4 the contour and spectrum of the vortex pair at the final stage are compared with those of the dipole vortex, eq.(2.21) with $a = 14.8$ and $c = -0.56$. The spectrum of the dipole vortex whose symmetry axis is at the angle of $\pi/4$ to the y axis is given as the sum of the spectrum of Fig.2.4(d) and that obtained by interchanging k_x and k_y in Fig.2.4(d), which is quite similar to the spectrum in Fig.2.4(b). Thus the dipole vortex at the final stage may be identified with the dipole vortex.

The amplitudes of the dipole vortex in the final stage are determined by assuming a stationary energy flow from the linearly unstable modes to the damped ones. Since the energy is mainly contained in $(k_x/k_0, k_y/k_0) = (\pm 1, 0), (0, \pm 1)$, and $(\pm 1, \pm 1)$ as is seen in Fig.2.5(a), we may look for stationary solutions of the truncated equation derived from eq.(2.23):

$$|\psi(1,0)|^2 \sim \frac{1}{4k_0^6}, \tag{2.33}$$

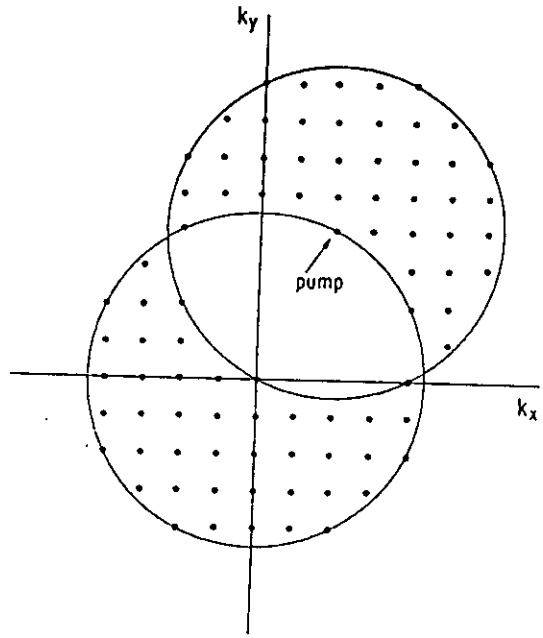

Figure 2.3: A set of wavenumbers subject to the parametric instability when the pump wave is taken to be $(k_x, k_y) = (2k_0, 4k_0)$.

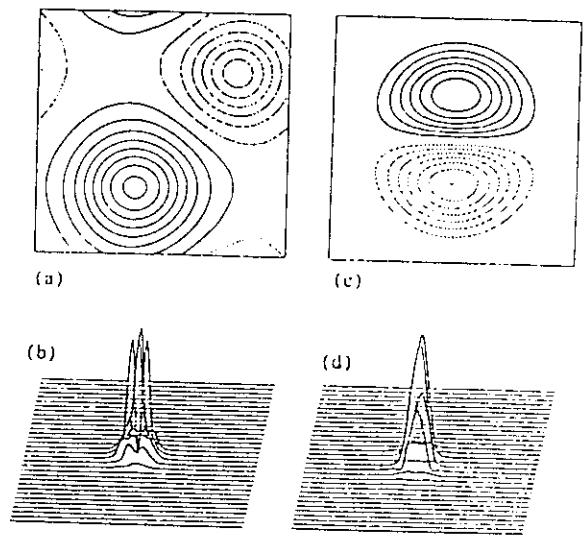

Figure 2.4: Spatial and spectral structures of the observed vortex pair and the stationary solution.(a) the contour of the potential observed at the final stage of the simulation for $\kappa = \nu = 0.3$ and $\delta = 0.1$, (b) the spectral structure for the case of (a), (c) the contour of the stationary solution for $a = 14.8$ and $c = -0.56$, and (d) the spectrum in the case of (d).

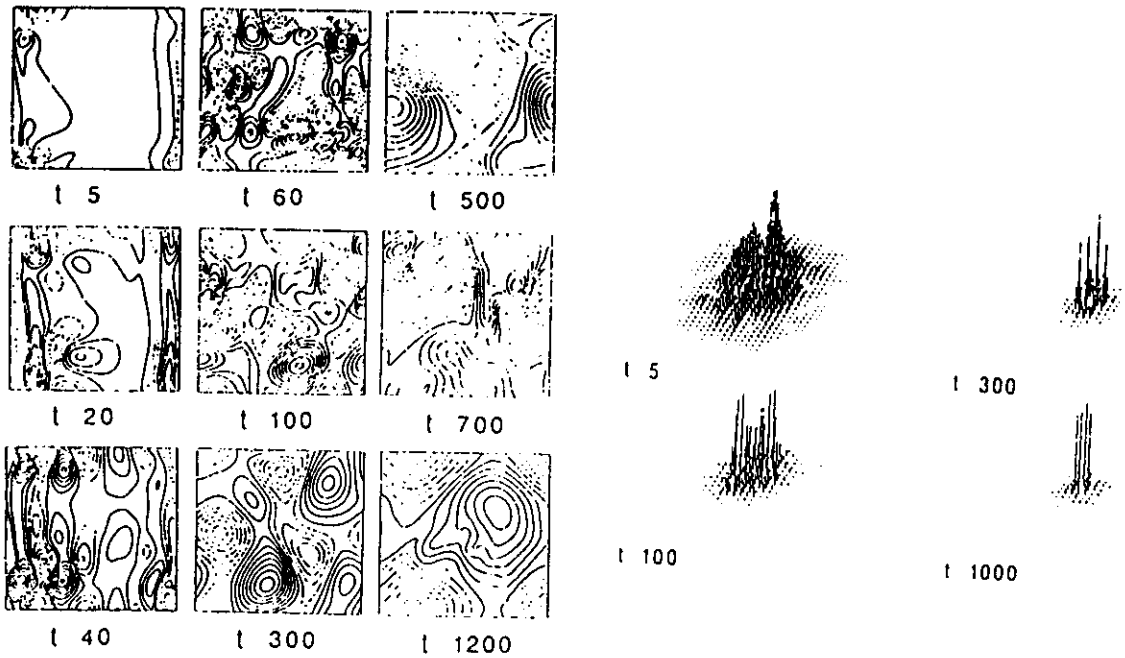

Figure 2.5: The time evolution of (a) the spatial structure and (b) the spectral structure of the potential for $\kappa = 0.4, \nu = 1.0$, and $\delta = 0.1$ when many waves are initially launched.

$$|\psi(0,1)|^2 \sim \frac{\nu\delta}{4k_0^3}, \tag{2.34}$$

$$|\psi(1,\pm 1)|^2 \sim \frac{\nu\delta}{2k_0^3}. \tag{2.35}$$

The magnitude of the amplitudes given by eqs.(2.33)-(2.35) is of the same order as that observed in the simulation. It is comparable to the saturation amplitude obtained by Terry and Horton [22] ($e\psi/T_e \sim 10/\varepsilon, \varepsilon = \rho/L_n$), which is claimed too high by Biskamp and Kaifen [9]. The reason for this might be related to the neglect of the coupling with ion acoustic waves [9].

Then many waves are initially launched for the parameters $\kappa = 0.4, \nu = 1.0$, and $\delta = 0.1$, small scaled vortices are readily formed since the linear instability is dominated in the initial stage of the evolution. The wave number spectrum of the potential resembles that of the linear growth rate. Apparently the parametric instability cannot be identified. The fusion of smaller vortices into larger ones becomes the main process of the evolution. The time developments of the potential and the wave spectrum are shown in Figs.2.5(a) and (b).

2.3 Discussion

We have studied the formation of a coherent structure through turbulence in the course of nonlinear development of the collisional drift wave instability. We derive a model equation which is the Hasegawa-Mima equation with the effect of collision and viscosity. The linear instability is followed by a parametric

instability to allocate the wave energy to many waves which, in turn, cause the destruction of the sinusoidal wave pattern into a random ensemble of small vortices. The small vortices are then fused to form larger vortices because of an inverse cascade. The fusion process is repeated to give a single large dipole vortex identified as a stationary solution of the Hasegawa-Mima equation.

Although many efforts have been devoted to establishing a scenario for nonlinear development of the drift wave instability, so far the scenario is terminated by the saturation of the instability and the resultant turbulence. Here we find that there is another stage beyond the turbulence state, that is, the onset and development of self-organized motions. In conclusion, the Hasegawa-Mima equation seems capable of describing a variety of nonlinear wave dynamics.

References

[1] A. Hasegawa and K. Mima, Phys. Fluids **21**, 87 (1978)

[2] C. M. Surko and R. E. Slusher, Phys. Rev. Lett. **40**, 400 (1978)

[3] A. Hasegawa and M. Wakatani, Phys. Rev. Lett. **50**, 682 (1983)

[4] D. Fyfe and D. Montgomery, Phys. Fluids **22** 246 (1979)

[5] R. H. Kraichnan, Phys. Fluids **10**, 1417 (1967)

[6] J. D. Meiss and W. Horton, Phys. Fluids **25**, 1838 (1982)

[7] H. Tasso, Phys. Lett. **96A**, 33 (1983)

[8] P. W. Terry and C. W. Horton, Phys. Fluids **25**, 491 (1982)

[9] D. Biskamp and H. Kaifen, Phys. Fluids **28**, 2172 (1985)

[10] W. W. Lee, J. A. Krommes, C. Oberman and R. Smith, Phys. Fluids **27**, 2652 (1984)

[11] A. Hasegawa, C. G. Maclennan and Y. Kodama, Phys. Fluids **22**, 2122 (1979)

[12] J. C. McWilliams, G. R. Flierl, V. D. Larichev and G. M. Reznik, Dyn. Atmos. Oceans **5**, 219 (1981)

[14] M. Makino, T. Kamimura and T. Taniuti, J. Phys. Soc. Jpn **50**, 980 (1981)

[15] C. E. Seyler Jr., Y. Sale, D. Montgomery and G. Knorr, Phys. Fluids **18**, 803 (1983)

[16] D. Montgomery, L. Turner and G. Vahala, Phys. Fluids **21**, 757 (1978)

[17] W. H. Matthaeus and D. Montgomery, Ann. NY Acad. Sci. **357**, 203 (1980)

[18] M. Hossain, G. Vahala and D. Montgomery, Phys. Fluids **28**, 3074 (1985)

[19] S. J. Braginskii, in *Reviews of Plasma Physics*, ed. by M. A. Leontvich (Consultant Bureau, New York, 1965), Vol.1, p.205

[20] J. D. Meiss and W. Horton, Phys. Fluids **26**, 990 (1983)

[21] W. Horton, in *Basic Plasma Physics*, ed. by A. A. Galeev and R. N. Sudan (North-Holland, Amsterdam, 1984), Vol.2, p.384

[22] A. R. Gourlay and J. L. Moris, J. Comput. Phys. **5**, 299 (1970)

[23] P. W. Terry and W. Horton, Phys. Fluids **26**, 106 (1983)

Chapter 3

Scenarios of self-organization

The emergence of organized states in turbulence was initiated by Montgomery and has been intensively studied by his group [1-11]. Through those efforts the scenarios of self-organization were almost established as long as two dimensional turbulence in fluids and plasmas is concerned. These are the selective decay hypothesis and maximal entropy principle. However transient dynamical properties such as a decay of the number of vortices is not understood by the scenarios. In this chapter we review the scenarios of self-organization and give a scaling theory to describe a transient process like a decay in the number of vortices.

3.1 Equations for two dimensional dynamics

First we derive equations describing dynamics of two dimensional fluids and plasmas. For ideal fluids we have as the equation of vorticity $\omega = \nabla \times \mathbf{v}$,

$$\frac{\partial}{\partial t}\omega + \mathbf{v} \cdot \nabla\omega = 0, \tag{3.1}$$

where ϕ is a stream function and velocity is given by $\mathbf{v} = \mathbf{z} \times \nabla\phi$. This equation is rewritten as

$$\frac{\partial}{\partial t}\nabla^2\phi + [\phi, \nabla^2\phi] = 0, \tag{3.2}$$

where $[\cdots, \cdots]$ is a Poisson bracket. It should be noted that since ϕ is a Hamiltonian, any ω expressed as an arbitrary function of ϕ is a stationary solution, implying there are infinite number of invariants. Among them physical invariants are energy E and enstrophy Ω:

$$E = \frac{1}{2}\int d\mathbf{r}\ v^2 = \sum |v(\mathbf{k}, t)|^2, \tag{3.3}$$

$$\Omega = \frac{1}{2}\int d\mathbf{r}\ \omega^2 = \sum k^2 |v(\mathbf{k}, t)|^2. \tag{3.4}$$

For electron plasmas we start with the electron continuity equation

$$\frac{\partial n}{\partial t} + \nabla(n\mathbf{v}) = 0, \tag{3.5}$$

the electron cross field velocity

$$\mathbf{v} = \frac{c}{B_0}\mathbf{z} \times \nabla(\phi - \frac{T}{e}\ln n), \tag{3.6}$$

and the Poisson equation

$$\nabla^2\phi = 4\pi en, \tag{3.7}$$

which are combined to give

$$\frac{\partial}{\partial t}\nabla^2\phi + [\phi, \nabla^2\phi] = 0. \tag{3.8}$$

This is exactly the same as that for two dimensional Euler equation (referred to as 2DNS equation in the following).

For low frequency fluctuations in plasmas, we start with equations for ion continuity and ion cross filed velocity, and the Poisson equation where electrons obey the Boltzmann distribution:

$$\frac{\partial n}{\partial t} + \nabla(n\mathbf{v}) = 0, \tag{3.9}$$

$$\mathbf{v} = \frac{c}{B_0}\mathbf{z} \times \nabla\phi, \tag{3.10}$$

$$\nabla^2\phi = 4\pi e(n_0 e^{e\phi/T} - n), \tag{3.11}$$

from which we have

$$\frac{\partial}{\partial t}(\kappa^2 - \nabla^2)\phi - \mathbf{v}_* \cdot \nabla\phi - [\phi, \nabla^2\phi] = 0,$$

$$\kappa = \frac{C_s}{\lambda_D\Omega}, \quad \mathbf{v}_* = \kappa^2\mathbf{z} \times \nabla \ln n_0. \tag{3.12}$$

Here κ denotes a screening effect by the electrons and $\mathbf{v}_*$ is a diamagnetic drift velocity due to an inhomogeneous background density. This equation is often referred to as the Charney-Hasegawa-Mima equation (CHM equation). Invariants are given by

$$E = \frac{1}{2}\int dr\{\kappa^2\phi^2 + (\nabla\phi)^2\} = \sum(\kappa^2 + k^2)|\phi(\mathrm{k}, t)|^2, \tag{3.13}$$

$$\Omega = \frac{1}{2}\int dr\{\kappa^2(\nabla\phi)^2 + (\nabla^2\phi)^2\} = \sum k^2(\kappa^2 + k^2)|\phi(\mathrm{k}, t)|^2. \tag{3.14}$$

For dynamical systems with several invariants all of the invariants are not necessarily relevant. Some of them are poorly conserved when infinitesimally small dissipation is introduced. Then the most probable state may be obtained by extremizing the poorly conserved invariants subject to the constraint that relevant invariants are kept constant.

3.2 Selective decay hypothesis

In order to distinguish relevant invariants from irrelevant ones, suppose that a system is in an equilibrium state. Then the probability distribution function of the stationary state is expressed in terms of invariants as

$$P(|v(\mathrm{k}_j)|^2, j = 1, 2, ...) = Ce^{-\alpha E - \beta\Omega}$$

$$= Ce^{-\sum(\alpha + \beta k^2)|v(\mathrm{k})|^2},$$

where α and β are Lagrangean multipliers. From this an expectation value of the energy spectrum is calculated as

$$< |v(\mathrm{k})|^2 >= \frac{1}{\alpha + \beta k^2}. \tag{3.15}$$

Here α and β are determined from expectation values of $< E >$ and $< \Omega >$:

$$< E > = \frac{1}{2}\sum \frac{1}{\alpha + \beta k^2}, \tag{3.16}$$

$$< \Omega > = \frac{1}{2}\sum \frac{k^2}{\alpha + \beta k^2}. \tag{3.17}$$

For a large system we have

$$< E > = 2\pi \int_{k_{min}}^{k_{max}} \frac{k}{\alpha + \beta k^2} dk = \frac{1}{2\beta} \log |\frac{\alpha + \beta k_{max}^2}{\alpha + \beta k_{min}^2}|, \tag{3.18}$$

$$< \Omega > = 2\pi \int_{k_{min}}^{k_{max}} \frac{k^3}{\alpha + \beta k^2} dk = \frac{1}{2\beta}[k_{max}^2 - k_{min}^2 - 2\alpha < E >]. \tag{3.19}$$

The effective temperature α and β could be negative, but not both simultaneously since $\alpha + \beta k^2 > 0$. In order to determine which could be negative, let k_{max} go to infinity for fixed $< E >$ and $< \Omega >$ [1]. Then from eq.(3.19) β becomes infinity and from eq.(3.18) which is rewritten as

$$\alpha = -\beta \frac{k_{min}^2 e^{2\beta < E >} - k_{max}^2}{e^{2\beta < E >} - 1},$$

we obtain

$$\alpha = -k_{min}^2 \beta.$$

Thus we have

$$< |v(\mathrm{k})|^2 >= \frac{1}{\beta} \frac{1}{k^2 - k_{min}^2}, \quad k_{min} = \sqrt{|\alpha|/\beta}. \tag{3.20}$$

This implies that the energy tends to concentrate at the longest allowed wavelength while since the extra factor of k^2 appears in the expression of the enstrophy:

$$< k^2 |v(\mathrm{k})|^2 >= \frac{k^2}{|\beta|} \frac{1}{k^2 - k_{min}^2}, \tag{3.21}$$

the enstrophy ranges up to k_{max} where dissipation becomes important.

So far we discuss a stationary spectrum distribution. When energy is supplied at a finite wavenumber which is between k_{min} and k_{max}, the energy cascades to a small wavenumber region (inverse cascade)and the enstrophy cascades to a larger wave number region (normal cascade). While the enstrophy cascades to a larger wavenumber and is dissipated strongly, the energy is almost conserved. This is the scenario for the selective decay of enstrophy. Thus we look for a state so as for the enstrophy to be minimum under the condition that the energy is constant. A variational problem is formulated as

$$\delta\Omega - \lambda\delta E = \delta \int [(\nabla^2\phi)^2 - \lambda(\nabla\phi)^2] dr = 0, \tag{3.22}$$

where λ is a Lagrange multiplier. This gives

$$\nabla^2\phi + \lambda\phi = 0, \tag{3.23}$$

which is nothing but one of the stationary solutions of eq.(3.2). The solution of eq. (3.23) is given by

$$\phi(\mathbf{r}) = \phi_0 \cos(k_x x)\cos(k_y y). \tag{3.24}$$

This state is characterized by a single wavenumber which is the smallest allowed by a boundary condition.

3.3 Maximal entropy principle

Maximal entropy principle is to determine a probable state from entropy. For that purpose we need discrete degrees of freedom which can be introduced by point vortices. Point vortices are defined through

$$\nabla^2\phi = \sum_j \gamma_j \delta(\mathbf{r} - \mathbf{r}_j(t)), \tag{3.25}$$

which is substituted into 2DNS equation to give

$$\frac{d}{dt}\mathbf{r}_j = \sum_\ell \gamma_\ell \frac{\mathbf{z}\times(\mathbf{r}_j - \mathbf{r}_\ell)}{|\mathbf{r}_j - \mathbf{r}_\ell|^2}. \tag{3.26}$$

The point vortex system is a Hamilton system which is confirmed by

$$\frac{dx_j}{dt} = \frac{1}{\gamma_j}\frac{\partial H}{\partial y_j}, \quad \frac{dy_j}{dt} = -\frac{1}{\gamma}\frac{\partial H}{\partial x_j}, \tag{3.27}$$

where

$$H = -\sum_{i\neq j}\gamma_i\gamma_j \ln|\mathbf{r}_i - \mathbf{r}_j|. \tag{3.28}$$

Since x and y are canonical conjugate in this system, the configuration space is nothing but the phase space. This is essentially different from ordinary Hamilton systems where the configuration space is a sub-space of the phase space. Suppose that the fluid enclosed by a boundary so that the vortices are confined to an area A. Then the volume of the phase space is given by

$$\int d\Omega = (\int dxdy)^N = A^N = finite. \tag{3.29}$$

On the other hand the energy of the system expressed by eq.(3.28) can range from $-\infty$ to ∞: when the vortices of the same sign coincide the energy becomes ∞, while when the vortices of the opposite sign coincide the energy becomes $-\infty$. The phase volume which corresponds to energy less than a given value E

$$H(x_1, y_1, \cdots, x_N, y_N) < E,$$

is a differentiable function of the energy:

$$\Psi(E) = \int_{H<E} d\Omega = \int_{-\infty}^{E} \Psi'(E)dE \tag{3.30}$$

with

$$\Psi(-\infty) = 0, \quad \Psi(\infty) = A^N. \tag{3.31}$$

The second condition comes from the fact that the vortices are confined in a finite area, the phase volume has to level off. Since $\Psi(E)$ is a monotonically increasing function of E and levels off for $E \to \infty$, $\Omega(E) = \Psi'(E)$ cannot increase monotonically and must have a negative slope for E larger than a finite E_m, that is, $\Psi'(E)$ is maximum at E_m and $\Omega'(E) < 0$ for $E > E_m$. From the definition of temperature

$$\frac{1}{T} = \frac{\partial S}{\partial E} = k_B \frac{\Omega'(E)}{\Omega(E)} = k_B \frac{\Psi''(E)}{\Psi'(E)}, \tag{3.32}$$

temperature is negative for $E > E_m$. In this region the entropy decreases with increasing E, that is, a higher level of organization corresponds to the higher energy state. For an equilibrium state characterized by the Boltzmann factor $exp(-E/k_BT)$, the state with the highest energy is most realizable since the temperature is negative. The state of the highest energy is realized when the same signed vortices come close together, which corresponds to the state with the highest order. Therefore vortices of the same sign will tend to cluster.

In order to determine a realizable state, let the entropy be maximize under the constraints that the energy and the number of vortices of positive and negative polarization are constant, which is formulated as follows

$$\delta \int d\mathbf{r}\{n_+ \log n_+ + n_- \log n_- + \alpha_+ n_+ + \alpha_- n_- + \beta\phi(\mathbf{r})(n_+ - n_-)\} = 0, \tag{3.33}$$

where α_+, α_-, and β are Lagrange multipliers. From this we have

$$n_\pm = e^{-\alpha} e^{\pm\beta\phi(\mathbf{r})},$$

where $1 + \alpha_+ = 1 + \alpha_- = \alpha$ has been used. Substituting these equations into the vorticity equation

$$\nabla^2\phi = \Gamma(n_+ - n_-), \quad \gamma_+ = \gamma_- = \Gamma,$$

a realizable state is given by

$$\nabla^2\phi + 2\Gamma e^{-\alpha} sinh(\beta\phi) = 0. \tag{3.34}$$

For small ϕ the above equation reduces to that given by the scenario of selective decal hypothesis. For large ϕ the difference becomes significant.

3.4 Test of scenarios

According to above mentioned scenarios a realizable state is given by either

$$\nabla^2\phi = -\lambda\phi, \tag{3.35}$$

or

$$\nabla^2\phi = -\kappa^2\phi + \lambda^2 \sinh(\beta\phi) \quad (\kappa = 0 \; for \; 2DNS). \tag{3.36}$$

The scenario can be checked by comparing a scatter plot of the vorticity $\nabla^2\phi$ versus the stream function ϕ given from numerical data with theoretical relations. This kind of check has been done by Seyler [13] who showed that maximal entropy principle gives better results than selective decay hypothesis in two dimensional turbulence.

3.5 Scaling theory of algebraic decay of the number of vortices

In the course of self-organization the number of vortices decreases algebraically,

$$N(t) = N_0(\frac{t}{\tau})^{-\xi}, \tag{3.37}$$

where the exponent ξ is given as nearly 1 for experiments on electron plasmas [12], 0.70 - 0.75 for numerical simulations on the 2DNS equation [9], and 0.4 - 0.5 for numerical simulations on the CHM equation [14].

For the 2DNS equation dimensional analysis gives

$$\phi \sim \frac{\ell^2}{t}, \tag{3.38}$$

where ℓ and t are a scale length and a characteristic time, respectively. Then the energy is expressed as

$$E = \int dr(\nabla\phi)^2 \sim \phi^2 \sim \frac{\ell^4}{t^2}, \tag{3.39}$$

Since the energy is conserved during the cascade process, we have

$$\ell \sim t^{1/2}. \tag{3.40}$$

The scale length ℓ can be regarded as an average inter-vortex distance, giving

$$N(t) \sim \ell^{-2} \sim t^{-1}, \tag{3.41}$$

which agrees well with the experimental result but differs a bit from numerical results.

For the CHM equation with a condition $\kappa >> k$, dimensional analysis gives

$$\phi \sim \kappa^2 \frac{\ell^4}{t}, \tag{3.42}$$

and

$$E = \int dr(\kappa^2\phi^2 + (\nabla\phi)^2) \sim \kappa^6 \frac{\ell^{10}}{t^2}. \tag{3.43}$$

Then this time we have again invoking the conservation of the energy

$$N(t) \sim \ell^{-2} \sim t^{-2/5}, \tag{3.44}$$

which fairly agrees with the numerical results.

References

[1] C.E.Seyler, Y.Salu, D.Montgomery and G.Knorr, *Phys. Fluids* 18,803 (1975)

[2] R.H.Kraichnan and D. Montgomery, *Repts. Progress in Physics* 43, 547 (1980)

[3] A.C.Ting, W.H.Matthaeus and D.Montgomery, *Phys. Fluids* 29, 3261 (1986)

[4] W.H.Matthaeus, W.T.Stribling, D.Martinez, S.Oughton and D.Montgomery, *Phys. Rev. Letters* **66**, 2731 (1991)

[5] D.Montgomery, *Phys. Letters* **39A**, 7 (1972)

[6] G. Joyce and D.Montgomery, *J. Plasma Phys.* **10**, 107 (1973)

[7] D. Montgomery and G. Joyce, *Phys. Fluids* **17**, 1139 (1974)

[8] A.C.Ting, H.Chen and Y.C.Lee, *Physica* **D26**, 37 (1987)

[9] J.C.McWilliams, *J. Fluid Mech.* **219**, 316 (1990)

[10] D. Montgomery, *Phys. Rev.* **A44**, 8437 (1991)

[11] R.A.Smith, *Phys. Rev.* **A43**, 1126 (1991)

[12] G.L.Eyink and H.Spohn, *J. Stat. Phys.* **70**, 833 (1993)

[13] C.E.Seyler, *J. Plasma Phys.* **56**, 533 (1996)

[14] T.Watanabe, H.Fujisaka and T.Iwayama, *Phys. Rev.* **E55**, 5575 (1997)

Chapter 4

Point vortex description of drift wave vortex dynamics

Studies on dynamics of drift wave vortices have mainly been performed numerically based on the Hasegawa-Mima equation [1] which is difficult to solve analytically. In this chapter we derive point vortex equations of motion for the vortex core in the point vortex limit from the Hasegawa-Mima equation and study the elementary processes of interaction of the vortices, through the ordinary dynamical equations. The dynamical equations for the interacting vortex cores provide a clear understanding of the dynamical properties of drift wave vortices as well as stationary properties of the associated plasma transport.

An advantage of introducing point vortices is to convert a nonlinear partial differential equation into a system of ordinary differential equations which are easier to solve, while wave phenomena are neglected. A crucial difference of the Hasegawa-Mima equation from Euler's equation is the existence of the drift term giving rise to dispersive waves, which requires that the vorticity attached to each point vortex no longer be constant but to vary in space and time, in contrast with the point vortex description of Euler's equation characterized by constant strength vorticities. This modulated point vortex model was first introduced by Kono and Yamagata [2] based on the fact that the Hasegawa-Mima equation conserves the vorticity along the trajectory, then later by Zabusky and McWilliams [3] who studied the configurations of the vortices corresponding to a stationary solution of the Hasegawa-Mima equation and stability of the configurations.

In Sec. 4.1 we rederive the point vortex equation for the Hasegawa-Mima equation. In Sec.4.2 an exact solution for a vortex pair is obtained and is shown to recover the dynamical properties of the drift wave vortices revealed by numerical simulations. In Sec.4.3 collision processes of two vortex pairs are studied. In Sec.4.4 a statistical theory of a many-vortex system is formulated where the vortex diffusion coefficient is analytically derived to give the empirical formula given by Horton [4]. Discussions are given in the last section.

4.1 Point vortex model

Starting with the Hasegawa-Mima equation

$$\frac{\partial \psi}{\partial t} + [\psi, \pi] + v_* \frac{\partial \psi}{\partial y} = 0, \tag{4.1}$$

where [,] denotes the Poisson bracket and

$$\pi = \psi - \nabla^2 \psi, \tag{4.2}$$

we introduce the vortices through

$$\pi(\mathrm{r}, t) = \sum_\alpha \kappa_\alpha(t) V_\alpha(\mathrm{r} - \mathrm{r}_\alpha(t)), \tag{4.3}$$

where $V_\alpha(\mathrm{r} - \mathrm{r}_\alpha(t))$ is a localized function at $\mathrm{r} = \mathrm{r}_\alpha(t)$ and $\mathrm{r}_\alpha(t)$ is determined by the characteristics of eq.(4.1);

$$\frac{d\mathrm{r}_\alpha(t)}{dt} - [\psi(\mathrm{r}_\alpha, t), \mathrm{r}_\alpha] = 0. \tag{4.4}$$

Substituting eq.(4.3) into eq.(4.1), we obtain

$$\sum_\alpha \{\frac{d\kappa_\alpha(t)}{dt} - \kappa_\alpha(t) \nabla \cdot (\frac{d\mathrm{r}_\alpha}{dt} - \mathbf{z} \times \nabla \psi(\mathrm{r}, t))\} V_\alpha(\mathrm{r} - \mathrm{r}_\alpha(t)) = -v_* \frac{\partial}{\partial y} \psi(\mathrm{r}, t). \tag{4.5}$$

Since $V_\alpha(\mathrm{r} - \mathrm{r}_\alpha(t))$ is a function localized around $\mathrm{r} = \mathrm{r}_\alpha(t)$, we may replace the arguments r appearing in the coefficients of $V_\alpha(\mathrm{r} - \mathrm{r}_\alpha)$ with $\mathrm{r}_\alpha(t)$, and then the second term of the left-hand side of eq.(4.5) vanishes according to eq.(4.4). Then we have

$$\sum_\alpha \frac{d\kappa_\alpha(t)}{dt} V_\alpha(\mathrm{r} - \mathrm{r}_\alpha(t)) = -v_* \frac{\partial}{\partial y} \psi(\mathrm{r}, t). \tag{4.6}$$

Multiplying both sides of eq.(4.6) by $V_\ell(\mathrm{r} - \mathrm{r}_\ell(t))$ and integrating with respect to r, where we may approximate the overlap integral as follows:

$$\int d\mathrm{r} V_\alpha(\mathrm{r} - \mathrm{r}_\alpha(t)) V_\ell(\mathrm{r} - \mathrm{r}_\ell(t)) \simeq \delta_{\alpha\ell}, \tag{4.7}$$

then we obtain

$$\frac{d\kappa_\alpha}{dt} = v_* \frac{dx_\alpha}{dt}. \tag{4.8}$$

When the localized function $V_\alpha(\mathrm{r} - \mathrm{r}_\alpha(t))$ is approximated by a delta function $\delta(\mathrm{r} - \mathrm{r}_\alpha(t))$, that is, the vortex is assumed a point vortex, we have from eqs.(4.2) and (4.3)

$$\psi(\mathrm{r}, t) = \frac{1}{2\pi} \sum_\alpha \kappa_\alpha(t) K_0(|\mathrm{r} - \mathrm{r}_\alpha(t)|), \tag{4.9}$$

where K_0 is the modified Bessel function of the second kind. In the following v_* is assumed possitive and constant:

$$\kappa_\alpha(t) = \kappa_{\alpha,0} + v_* x_\alpha(t), \tag{4.10}$$

where $\kappa_{\alpha,0}$ is a constant. Then eq.(4.4) becomes

$$\frac{d\mathbf{r}_\alpha}{dt} = \frac{1}{2\pi}\sum_{\beta\neq\alpha}(\kappa_{\beta 0} + v_* x_\beta)\mathbf{z}\times\nabla_\beta K_0(r_{\alpha\beta}), \tag{4.11}$$

where $r_{\alpha\beta} = |\mathbf{r}_\alpha - \mathbf{r}_\beta|$. Equation has the same form as that introduced by Kono and Yamagata first and then later by Zabusky and McWilliams who introduced the name modulated point vortex for the variation $\kappa_\alpha = \kappa_{\alpha 0} + v_* x_\alpha$. The simple case of constant κ_α valid when $v_* = 0$ is studied by Hasegawa et al [5].

There are two conserved quantities for the Hasewgawa-Mima equation; one is the energy

$$E = \frac{1}{2}\int d\mathbf{r}[\psi^2 + (\nabla\psi)^2] = \frac{1}{2}\int d\mathbf{r}\psi\pi, \tag{4.12}$$

and the other is the enstropy

$$W = \frac{1}{2}\int d\mathbf{r}[(\nabla\psi)^2 + (\nabla^2\psi)^2] = -\frac{1}{2}\int d\mathbf{r}(\nabla^2\psi)\pi. \tag{4.13}$$

In the point vortex description the energy and enstrophy are expressed as

$$E = \frac{1}{4\pi}\sum_{\alpha\neq\beta}(\kappa_{\alpha 0} + v_* x_\alpha)(\kappa_{\beta 0} + v_* x_\beta)K_0(r_{\alpha\beta}), \tag{4.14}$$

$$W = \frac{1}{8\pi}\sum_{\alpha\neq\beta}(\kappa_{\alpha 0} + v_* x_\alpha)(\kappa_{\beta 0} + v_* x_\beta)[K_0(r_{\alpha\beta}) + K_2(r_{\alpha\beta})], \tag{4.15}$$

where the self-energy has been subtracted since it diverges. Although eqs.(4.14) and (4.15) are not conserved in general since

$$\frac{dE}{dt} = -\frac{1}{2}\sum_\alpha v_*\frac{\partial}{\partial y_\alpha}v^2(\mathbf{r}_\alpha, t), \tag{4.16}$$

and

$$\frac{dW}{dt} = -\frac{1}{2}\sum_\alpha v_*\frac{\partial}{\partial y_\alpha}[\nabla v(\mathbf{r}_\alpha, t)]^2, \tag{4.17}$$

this does not mean that the point vortex description is invalid. The discrepancy comes from the fact eqs.(4.12) and (4.13) take into account contributions from both vortices and waves, while eqs.(4.14) and (4.15) are based on vortices only. Therefore for the vortex pairs corresponding to the stationary solution of the Hasegawa-Mima equation, that is, for those propagating straight in the y direction, eqs.(4.14) and (4.15) are certainly constants of motion since the waves are never excited. In general, however, changes in energy and enstropy of the vortex system in the course of time evolution may occur whenever waves are involved in the fundamental processes of the vortices such as emission or absorption of waves by the vortices, which is observed in numerical experiments [6,7] based on the Hasegawa-Mima equation.

Equation (4.14) is not a Hamiltonian of the dynamical system of the vortices. Instead the Hamiltonian is given by

$$H = \sum_\alpha v(\mathbf{r}_\alpha, t). \tag{4.18}$$

from which we have

$$\frac{dx_\alpha}{dt} = -\frac{\partial H}{\partial y_\alpha} = \frac{1}{2\pi}\sum_\beta (\kappa_{\beta 0} + v_* x_\beta)\frac{y_\alpha - y_\beta}{r_{\alpha\beta}} K_1(r_{\alpha\beta}), \tag{4.19}$$

$$\frac{dy_\alpha}{dt} = \frac{\partial H}{\partial x_\alpha} = -\frac{1}{2\pi}\sum_\beta (\kappa_{\beta 0} + v_* x_\beta)\frac{x_\alpha - x_\beta}{r_{\alpha\beta}} K_1(r_{\alpha\beta}). \tag{4.20}$$

Since H is translationally invariant along the y axis, the translational momentum in x is conserved:

$$P = \sum_\alpha (\kappa_{\alpha 0} + v_* x_\alpha)^2. \tag{4.21}$$

4.2 Vortex-pair solution

Now we solve eqs.(4.19) and (4.20) for two vortices. In this case, in addition to eq.(4.21), the relative distance of the vortices is a constant of motion,

$$r_{12}^2 = (x_1 - x_2)^2 + (y_1 - y_2)^2 = r_0^2, \tag{4.22}$$

which leads to

$$\frac{d}{dt}\cos\theta = \pm\frac{v_* K_1(r_0)}{2\pi}\sqrt{(A + \cos\theta)(B - \cos\theta)(1 - \cos^2\theta)}, \tag{4.23}$$

where $x_1 - x_2 = r_0\cos\theta$, $A = |\sqrt{2P} + (\kappa_{20} - \kappa_{10})|/v_* r_0$, and $B = |\sqrt{2P} - (\kappa_{20} - \kappa_{10})|/v_* r_0$. Equation (4.22) is readily integrated to yield a solution expressed in terms of the Jacobi elliptic function. The solution is given by

$$\cos\theta = \gamma\frac{1 - \beta^2 sn^2(\omega t, k)}{1 - a^2 sn^2(\omega t, k)}, \tag{4.24}$$

where for $v_* r_0 + |\kappa_{10} - \kappa_{20}| > \sqrt{2P} > |v_* r_0 - |\kappa_{10} - \kappa_{20}||$,

$$a^2 = \frac{1 + B}{A + B},\ \beta^2 = Aa^2, \tag{4.25}$$

$$\gamma = -sgn(\kappa_{10} - \kappa_{20}), \tag{4.26}$$

$$\omega = \sqrt{2(A + B)}\frac{v_* K_1(r_0)}{4\pi}, \tag{4.27}$$

$$k = \sqrt{(1 + A)(1 + B)/2(A + B)}, \tag{4.28}$$

and for $\sqrt{2P} < |v_* r_0 - |\kappa_{10} - \kappa_{20}||$,

$$a^2 = \frac{A + B}{1 + B},\ \beta^2 = a^2/A, \tag{4.29}$$

$$\gamma = -Asgn(\kappa_{10} - \kappa_{20}), \tag{4.30}$$

$$\omega = \sqrt{(1 + A)(1 + B)}\frac{v_* K_1(r_0)}{4\pi}, \tag{4.31}$$

$$k = \sqrt{2(A + B)/|(1 + A)(1 + B)|}. \tag{4.32}$$

Equations for the center of gravity are given by

$$\frac{1}{2}(x_1 + x_2) = -\frac{\pi r_0}{v_*}K_1(r_0)\frac{d\theta}{dt} - \frac{\kappa_{10} + \kappa_{20}}{2v_*}, \tag{4.33}$$

$$\frac{1}{2}\frac{d}{dt}(y_1 + y_2) = \frac{K_1(r_0)}{4\pi}(\kappa_{10} - \kappa_{20} + v_* r_0\cos\theta)\cos\theta. \tag{4.34}$$

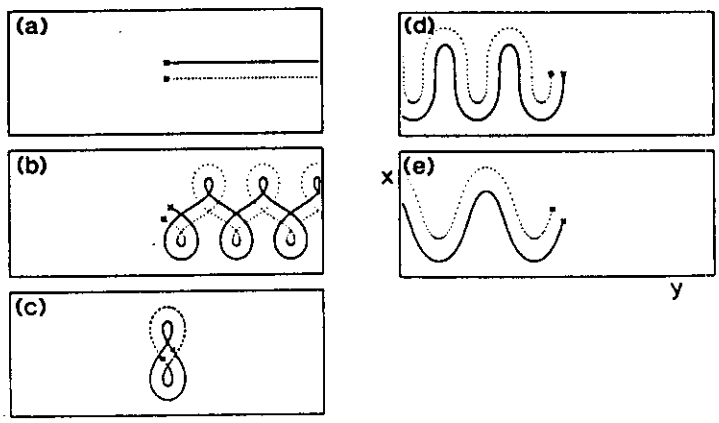

Figure 4.1: Trajectories of an opposite signed vortex pair of $\kappa/v_* = 2.0$ and $r_0 = 0.4$: solid lines and dotted lines indicate a positive and negative vortex, respectively. Angles θ_0 between the symmetry axis and the x axis are (a) 0, (b) $\pi/6$, (c) 0.8976, (d) $\pi/2$, and (e) $2\pi/3$.

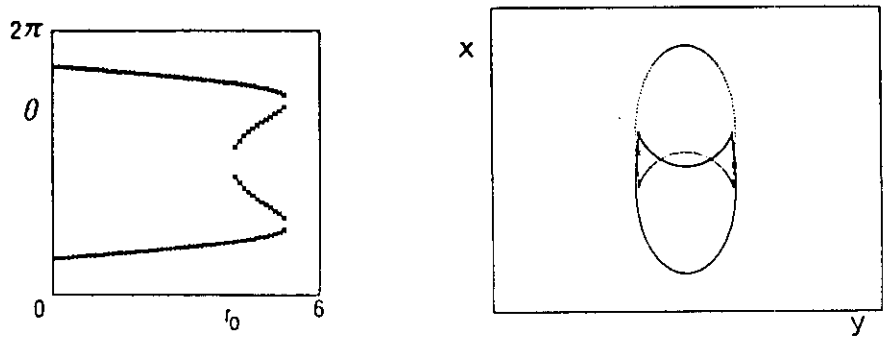

Figure 4.2: (a) Tilted angle versus the size of the vortex pair for non-propagating vortex pair of $\kappa/v_* = 2.0$, and (b) non-propagating vortex pair of $\kappa/v_* = 2.0, r_0 = 5.0$ and $\theta_0 = 1.6755$.

whose explicit solutions are readily obtained by using eq.(4.24).

It must be noted that a vortex pair ($\kappa_{10} + \kappa_{20} = 0$) propagates in the y direction without oscillation in the orbit $\theta_0 (= \theta(t = 0)) = n\pi$ (n:integer) and with oscillation for $\theta_0 \neq n\pi$ as is shown in Fig.4.1, which has been numerically observed by Makino et al [8] based on the Hasegawa-Mima equation. Computations are monitored by keeping P constant within ten effective figures. Recently, Nycander and Isichenko [9] derived the equation for the center of gravity of a vortex pair from the momentum equations of the Hasegawa-Mima equation and obtained the frequency of the trajectory which is also well fitted to the results by Makino et al. A non-propagating solution shown in Fig.4.1(c) is realized for such initial angles of the symmetry axis of the vortex pair to the axis that the velocity of the vortex pair given by

$$\frac{1}{2} < \frac{d}{dt}(y_1 + y_2) > = \frac{1}{8K(k)} \int_0^{4K(k)} dt \frac{K_1(r_0)}{2\pi} (\kappa_{10} - \kappa_{20} + v_* r_0 \cos\theta) \cos\theta, \tag{4.35}$$

$$= \sqrt{2P}(1 - 2\frac{E(k)}{K(k)}) \frac{K_1(r_0)}{4\pi} = c, \tag{4.36}$$

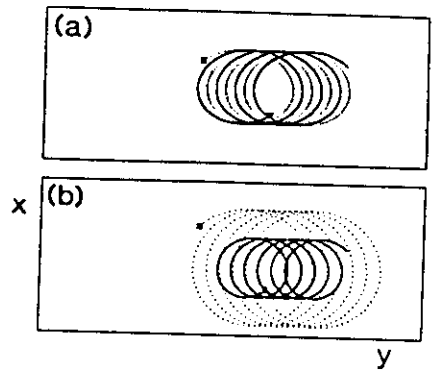

Figure 4.3: Trajectories of a like-signed vortex pair: (a) equal vorticitity strength $(\kappa_1, r_1) = (\kappa_2, r_2) = (20, 2)$ and (b) strong-weak vortices $(\kappa_1, r_1) = (50, 4)$ and $(\kappa_2, r_2) = (20, 2)$.

is zero where $K(k)$ and $E(k)$ are the complete elliptic integral of the first and second kind, respectively. Figure 4.2(a) shows the initial angle versus the size of the non-propagating vortex pairs for the case of $\kappa_0/v_* = 2.0$. Another example of a non-propagating vortex pair is given by Fig.4.2(b).

Two like-signed vortices ($\kappa_{10} = \kappa_{20}$) are mutually trapped, rotating around the center of gravity which is easily seen from eqs.(4.28) and (4.29) (Fig.4.3). This mutual trapping leads to a coarse graining of the correlation over directions and may be considered a mechanism behind the fusion of vortices in the sense that a group of point vortices positioned sufficiently near one another act at large distances as a single vortex with the sum intensity, $\kappa_T \simeq \Sigma_\alpha \kappa_\alpha$. A coalescence of like-vortices and a long-lived monopole numerically observed by Horton may be interpreted by this mutual trapping process. The inverse cascade of the energy is also regarded in the vortex representation as a trapping and as a kind of snowballing process.

4.3 Collision processes of two vortex pairs

Collision processes of two vortex pairs are shown to recover those observed numerically [6,7,10] for elastic cases with zero (Fig.4.4) and nonzero (Fig.4.5) impact parameters. Since our point vortex model does not take into account the effects of interaction with the wake fields, the inelastic collisions with an emission of wake fields observed by McWilliams and Zabusky [10] cannot be described by the vortex field component in eq.(4.9) alone. However, the position dependence of the vorticity gives the vortex system studied here a variety of complicated behaviors including an exchange scattering and a boomerang scattering (Fig.4.6), indicating that our point vortex system is likely to become turbulent when many vortices are involved. However, the potential structure constructed from eq.(4.9) is quite orderly as is shown in Fig.4.7, which corresponds to Fig.4.5; mutually trapped vortices behave as a single vortex though the dynamics of constituent point vortices is very complicated. Therefore the complication of the dynamics of the point vortices is rather analogous to complicated behaviors of constituent particles in an ordinary gas or fluid

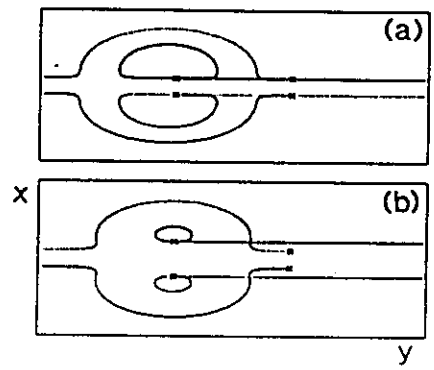

Figure 4.4: Head-on collision between two opposite signed vortex-pairs with zero impact parameter.

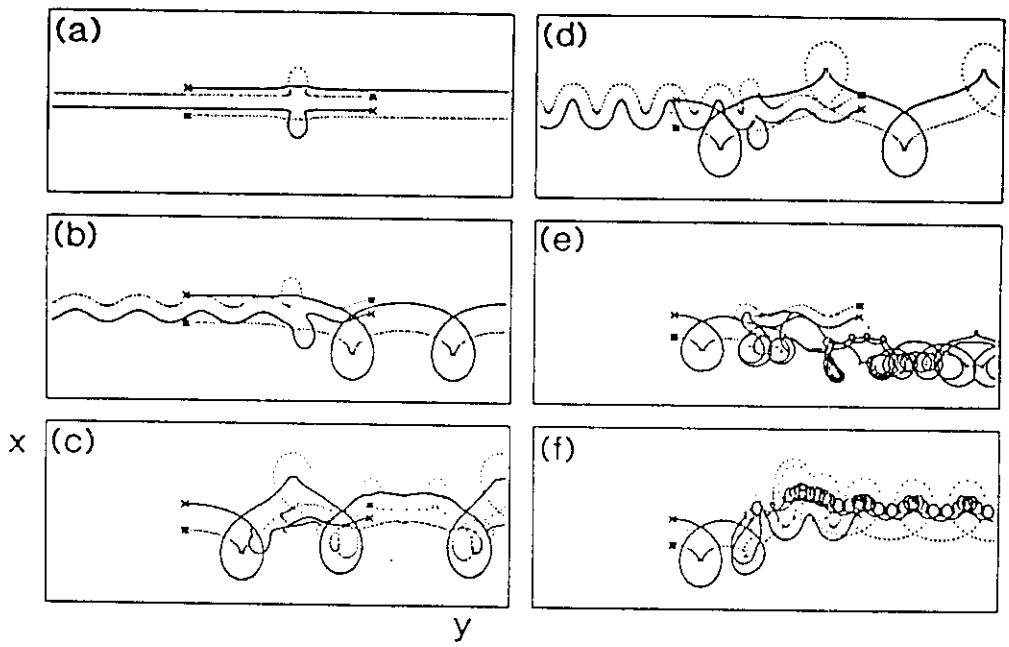

Figure 4.5: Head-on collision between two opposite signed vortex-pairs of $\kappa_1/v_* = -1.0, \kappa_2/v_* = 1.0, \kappa_3/v_* = 2.0$, and $\kappa_4/v_* =^2 .0$ with the initial positions: $x_1 = x_{10} + \Delta x_1, x_2 = -x_{10} + \Delta x_1, x_3 = x_{20} + \Delta x_2, x_4 = -x_{20} + \Delta x_2, x_{10} = 0.25, x_{20} = 0.50, y_1 = y_2 = -y_3 = -y_4 = 4.0$, with $(\Delta x_1, \Delta_2) = (a)(0.0, 0.0), (b)(0.15, 0.0), (c)(0.15, 0.15), (d)(0.25, 0.25), (e)(0.25, 0.50), (f)(0.50, 0.50)$.

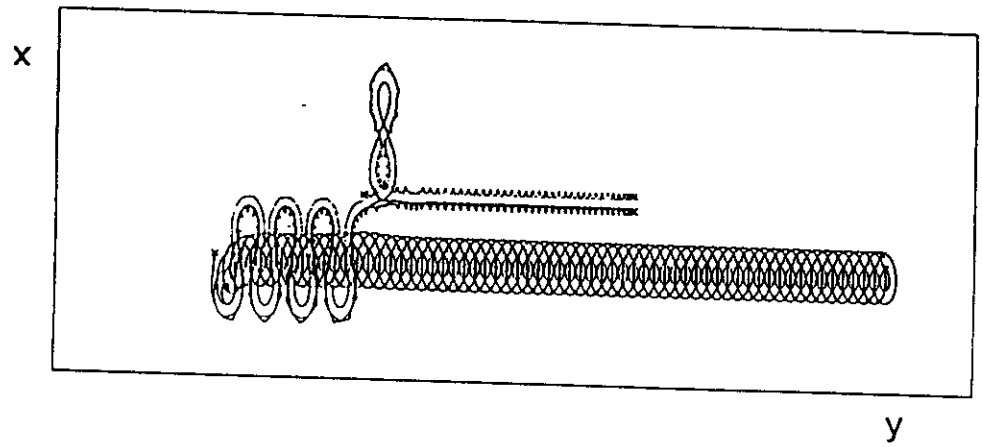

Figure 4.6: Trajectories of four vortices $\kappa/v_* = -\kappa_2/v_* = \kappa_3/v_* = -\kappa_4/v_* = -9.0$ with initial positions $x_1 = -x_2 = x_3 = -x_4 = 0.35, y_1 = y_2 = -y_3 = -y_4 = 0.2$.

dynamics and averaged properties may be of primary importance although the dynamical properties of the point vortex system are academically interesting since the chaotic behavior may be characterized by intermittent structures and clusters of vortices in which local order is a preferred state because of the short range interaction force between point vortices. The range of the interaction $\rho_s = c(m_i T_e)^{1/2}/eB$ is given by the parallel electron motion shielding the charge separation in the Euler vortex.

4.4 Vortex collapse revisited

When the diamagnetic drift is neglected the equations for the motion of vortices are given by

$$\frac{d}{dt}\mathrm{r}_\alpha = \frac{1}{2\pi}\sum_\beta \kappa_\beta \frac{\mathrm{z}\times(\mathrm{r}_\alpha - \mathrm{r}_\beta)}{|\mathrm{r}_\alpha - \mathrm{r}_\beta|} K_1(|\mathrm{r}_\alpha - \mathrm{r}_\beta|). \tag{4.37}$$

The short range nature of the interaction between the vortices stems from the shielding effect. This implies that the distance between the vortices is short enough for the shielding to be neglected, the dynamical behavior of vortices is described by the following equation:

$$\frac{d}{dt}\mathrm{r}_\alpha = \frac{1}{2\pi}\sum_\beta \kappa_\beta \frac{\mathrm{z}\times(\mathrm{r}_\alpha - \mathrm{r}_\beta)}{|\mathrm{r}_\alpha - \mathrm{r}_\beta|^2}, \tag{4.38}$$

which are the point vortex equations corresponding to Euler's equation. There are three conserved quantities associated with eq.(4.38),

$$\mathrm{G} = \sum_\alpha \kappa_\alpha \mathrm{r}_\alpha, \tag{4.39}$$

$$L = \sum_\alpha \kappa_\alpha |\mathrm{r}_\alpha|^2, \tag{4.40}$$

$$E = = \sum_\alpha \sum_\beta \kappa_\alpha \kappa_\beta K_0(|\mathrm{r}_\alpha - \mathrm{r}_\beta|). \tag{4.41}$$

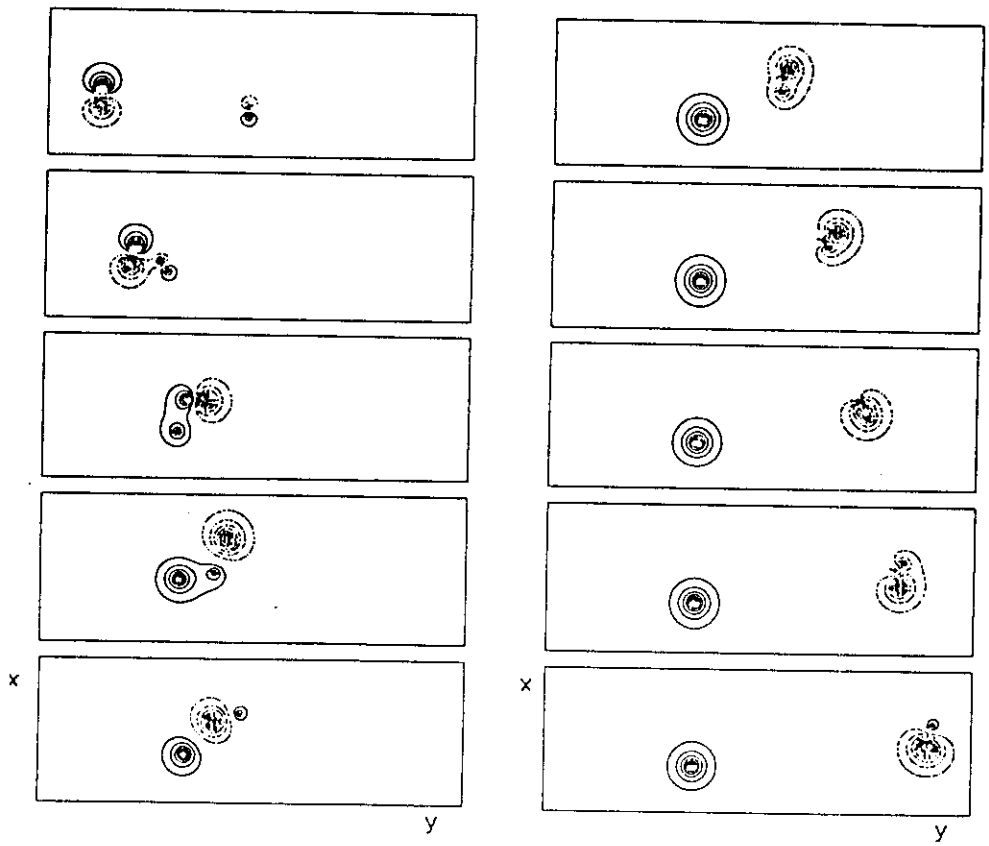

Figure 4.7: Contours of streamfunction obtained from eq.(4.9) using the point vortex trajectories in Fig.4.4(c).

Many studies [10,11] have been reported on solutions of eq.(4.38). Among them are also remarkable works concerned with the vortex collapse for which three vortices converge self-similarly. For the collapse to occur, suitable initial conditions have to be satisfied in addition to the condition that $\kappa_1\kappa_2+\kappa_2\kappa_3+\kappa_3\kappa_1 = 0$ [11]. Depending on the sign of vorticities κ_α, $\{\alpha = 1, 2 \text{ and } 3\}$ the vortices can also diverge [12]. This type of "explosive" motion can be considered as an "inversion" of the collapse.

The vortex collapse is algebraically unstable: a small deviation from the condition no longer leads to the collapse. In those cases three vortices first converge to some extent and then turn to diverge. Once they start to diverge, they keep diverging as long as eq.(4.38) is applicable. This is, however, not the case for eq.(4.37). When they diverge, two of them are to form a pair to travel together and the third one is left behind, because of the short range nature of the interaction. However since the vorticities of two vortices travelling together are opposite in sign and have to be different in magnitude, the two vortices perform a circular motion. They eventually return to the place where the third one remains. At the time they come to the position where the two sides of the triangle become equal, the pair is renewed by changing the partner. The new pair travels in a similar way as before until it comes back to the place and again, exchange its partner.

Introducing complex variables $z_\alpha = x_\alpha + iy_\alpha$ representing the vortex position $\mathbf{r}_\alpha = (x_\alpha, y_\alpha)$, eq.(4.37) is rewritten as

$$\frac{d}{dt}z_\alpha = \frac{i}{2\pi}\sum_\beta \kappa_\beta \frac{z_\alpha - z_\beta}{|z_\alpha - z_\beta|}K_1(|z_\alpha - z_\beta|). \tag{4.42}$$

With the aid of the cyclic permutation, the set of equations (4.42) for three vortices reduces to

$$\frac{d\rho}{dt} = -\frac{\kappa_1}{2\pi}[\eta\frac{K_1(\ell)}{\ell} - K_1(\eta)]\sin\Psi, \tag{4.43}$$

$$\frac{d\eta}{dt} = \frac{\kappa_2}{2\pi}[\rho\frac{K_1(\ell)}{\ell} - K_1(\rho)]\sin\Psi, \tag{4.44}$$

where

$$z_2 - z_3 = \rho e^{i\theta}, \quad z_3 - z_1 = \eta e^{i\phi}, \tag{4.45}$$

$$\Psi = \theta - \phi, \quad \ell = |z_1 - z_2| = \sqrt{\rho^2 + \eta^2 + 2\rho\eta\cos\Psi}.$$

From Eqs.(4.39) and (4.45), we have for $\kappa_1 + \kappa_2 + \kappa_3 \neq 0$

$$z_1 = -\frac{1}{\kappa_1+\kappa_2+\kappa_3}\{(\kappa_2+\kappa_3)\eta e^{i\phi} + \kappa_2\rho e^{i\theta} - G\}, \tag{4.46}$$

$$z_2 = \frac{1}{\kappa_1+\kappa_2+\kappa_3}\{\kappa_1\eta e^{i\phi} + (\kappa_1+\kappa_3)\rho e^{i\theta} + G\}, \tag{4.47}$$

$$z_3 = \frac{1}{\kappa_1+\kappa_2+\kappa_3}\{\kappa_1\eta e^{i\phi} - \kappa_2\rho e^{i\theta} + G\}. \tag{4.48}$$

The constants of motion L and E are now expressed by

$$L = \frac{1}{\kappa_1+\kappa_2+\kappa_3}\{\kappa_1\kappa_2\ell^2 + \kappa_2\kappa_3\rho^2 + \kappa_3\kappa_1\eta^2 + |G|^2\}, \tag{4.49}$$

$$E = \kappa_1\kappa_2 K_0(\ell) + \kappa_2\kappa_3 K_0(\rho) + \kappa_3\kappa_1 K_0(\eta). \tag{4.50}$$

With the use of eqs.(4.49) and (4.50), either eq.(4.43) or (4.44) is enough for obtaining the solution in principle. However eq.(4.50) is not convenient to use. Therefore we consider eqs.(4.43) and (4.44) with eq.(4.49).

First we review the collapse for which the modified Bessel function can be approximated as

$$K_0(x) \simeq -0.577 + \ln 2 - \ln x \quad for \quad x << 1. \tag{4.51}$$

For the collapse the solutions are self-similar in time and may be expressed in terms of $(\rho, \eta, \ell) = (\rho_0, \eta_0, \ell_0) f(t)$, for which the conserved quantities are given by

$$\begin{aligned} L &\propto [\kappa_1\kappa_2\ell_0^2 + \kappa_2\kappa_3\rho_0^2 + \kappa_3\kappa_1\eta_0^2] f(t)^2, \\ E &\simeq (\kappa_1\kappa_2 + \kappa_2\kappa_3 + \kappa_3\kappa_1) \ln |f(t)|. \end{aligned}$$

Therefore for the collapse to occur the following conditions have to hold:

$$L = 0 \quad and \quad \kappa_1\kappa_2 + \kappa_2\kappa_3 + \kappa_3\kappa_1 = 0, \tag{4.52}$$

where G is chosen to be zero. The first condition of eq.(4.52) is explicitly written as

$$\frac{\kappa_2}{\kappa_1 + \kappa_2}\rho_0^2 + \frac{\kappa_1}{\kappa_1 + \kappa_2}\eta_0^2 = \ell_0^2, \tag{4.53}$$

where ρ_0, η_0 and ℓ_0 are their initial values. Equation(4.53) gives the relation among the initial positions of the three vortices for the collapse to occur.

Then eqs.(4.43) and (4.44) become

$$\frac{d\rho}{dt} = -\frac{\kappa_1}{2\pi}\left(\frac{\eta}{\ell^2} - \frac{1}{\eta}\right)\sin\Psi, \tag{4.54}$$

$$\frac{d\eta}{dt} = \frac{\kappa_2}{2\pi}\left(\frac{\rho}{\ell^2} - \frac{1}{\rho}\right)\sin\Psi, \tag{4.55}$$

which are combined to give

$$\frac{d\rho}{d\eta} = \frac{\rho}{\eta}. \tag{4.56}$$

Thus we have

$$\frac{\rho}{\eta} = \frac{\rho_0}{\eta_0} \equiv \alpha. \tag{4.57}$$

For this case Ψ is also constant:

$$\cos\Psi = \frac{\kappa_3(\kappa_2 + \alpha^2\kappa_1)}{2\alpha\kappa_1\kappa_2}. \tag{4.58}$$

Then eq.(4.55) reduces to

$$\frac{d\eta}{dt} = \frac{(\alpha^2 - 1)\kappa_1\kappa_2}{2\pi\alpha(\kappa_1 + \alpha^2\kappa_2)\eta}\sin\Psi \equiv \frac{A}{\eta}, \tag{4.59}$$

which gives

$$\eta = \sqrt{\eta_0^2 + 2At}, \tag{4.60}$$

$$\rho = \alpha\eta, \tag{4.61}$$

$$\ell = \sqrt{-\frac{\kappa_3}{\kappa_1\kappa_2}(\kappa_1 + \alpha^2\kappa_2)}\,\eta. \tag{4.62}$$

From the imaginary part of $d(z_2 - z_3)/dt$ we have

$$\begin{aligned}\frac{d\theta}{dt} &= -\frac{1}{2\pi\rho}\{(\kappa_2+\kappa_3)K_1(\rho)+\kappa_1[\frac{\rho+\eta\cos\Psi}{\ell}K_1(\ell)-K_1(\eta)\cos\Psi]\}\\ &\simeq -\frac{1}{2\pi\rho}\{\frac{\kappa_2+\kappa_3}{\rho}+\kappa_1[\frac{\rho+\eta\cos\Psi}{\ell^2}-\frac{\cos\Psi}{\eta}]\}\\ &\equiv \frac{B}{\eta_0^2+2At},\end{aligned} \tag{4.63}$$

leading to

$$\theta = \frac{B}{2A}\ln|\frac{\eta_0^2+2At}{\eta_0^2}| + \theta_0, \tag{4.64}$$

where

$$B = -\frac{1}{2\pi\alpha}\{\frac{\kappa_1+\kappa_2}{\alpha}-\kappa_1[\frac{\kappa_1\kappa_2(\alpha+\cos\Psi)}{\kappa_3(\kappa_1+\alpha^2\kappa_2)}+\cos\Psi]\}. \tag{4.65}$$

Equations(4.60) - (4.64) give a self-similar solution which diverges or converges depending on the sign of A, that is, $\alpha^2 - 1$ except for the following two cases:

$$(a)\quad \alpha = \frac{1}{-\kappa_1\kappa_3}[\kappa_1\kappa_2 \pm \sqrt{-\kappa_1\kappa_2\kappa_3(\kappa_1+\kappa_2+\kappa_3)}], \tag{4.66}$$

$$(b)\quad \alpha = 1, \tag{4.67}$$

The case (a) comes from $\sin\Psi = 0$. The both cases correspond to a rigid rotation.

4.5 Boomerang interaction of three vortices

Now we relax one of the conditions for the collapse given by eq.(4.52), that is,

$$L \neq 0 \quad and \quad \kappa_1\kappa_2 + \kappa_2\kappa_3 + \kappa_3\kappa_1 = 0. \tag{4.68}$$

First, in order to see the effect of eq.(4.68) on the converging collapse solution, we may use the approximate expression eq.(4.51) for the vortices with short distances. Under the conditions eq.(4.68), the conserved quantities eqs.(4.49) and (4.50) are rewritten as

$$\kappa_1\kappa_2\ell^2 + \kappa_2\kappa_3\rho^2 + \kappa_3\kappa_1\eta^2 = \varepsilon, \tag{4.69}$$

$$(\frac{\ell}{\ell_0})^{\kappa_1\kappa_2}(\frac{\rho}{\rho_0})^{\kappa_2\kappa_3}(\frac{\eta}{\eta_0})^{\kappa_3\kappa_1} = 1, \tag{4.70}$$

where $\varepsilon = (\kappa_1+\kappa_2+\kappa_3)L$ and G is chosen zero. The ℓ_0, ρ_0 and η_0 are their initial values, respectively. For simplicity, in the following, we consider a special case:

$$(\kappa_1, \kappa_2, \kappa_3) = (\kappa, \kappa, -\kappa/2), \tag{4.71}$$

which satisfies one of the conditions given by eq.(4.68). Then eq.(4.70) simply becomes

$$\frac{\ell^2}{\rho\eta} = \frac{\ell_0^2}{\rho_0\eta_0} = C. \tag{4.72}$$

which is combined with eqs.(4.69) and (4.45) to give

$$\rho^2+\eta^2-2C\rho\eta+\frac{2\varepsilon}{\kappa^2}=0, \tag{4.73}$$

$$\cos\Psi=\frac{\ell^2-\rho^2-\eta^2}{2\rho\eta}=-\frac{C}{2}+\frac{\varepsilon}{\kappa^2\rho\eta}. \tag{4.74}$$

Then from eqs.(4.54),(4.55) and (4.72) we have

$$\frac{d}{dt}\ell^2=\pm\frac{\kappa}{2\pi\ell^4}\{(C^2-1)(4-C^2)(\ell^2-\ell_1^2)(\ell^2-\ell_2^2)(\ell^2-\ell_3^2)(\ell^2-\ell_4^2)\}^{1/2}, \tag{4.75}$$

where

$$\{\ell_1^2,\ell_2^2,\ell_3^2,\ell_4^2\}=\{\frac{C}{C-1}\frac{\varepsilon}{\kappa^2},\frac{C}{C+1}\frac{\varepsilon}{\kappa^2},\frac{2C}{2+C}\frac{\varepsilon}{\kappa^2},\frac{2C}{C-2}\frac{\varepsilon}{\kappa^2}\}, \tag{4.76}$$

with

$$\ell_1>\ell_2>\ell_3>\ell_4. \tag{4.77}$$

Equation (4.75) gives the same solution as eqs.(4.60), (4.61) and (4.62) for $\varepsilon=0$. The solution to eq.(4.75) is given by

$$\ell_1^4 g(\frac{\beta_1}{\beta})^4\{V_0+2\frac{\beta^2-\beta_1^2}{\beta_1^2}V_1+\frac{(\beta^2-\beta_1^2)^2}{\beta^4}V_2\}=\pm\frac{\kappa}{2\pi}\sqrt{(C^2-1)(4-C^2)}t, \tag{4.78}$$

where

$$\begin{aligned}
V_0 &= F(\phi,k),\quad V_1=\Pi(\phi,\beta^2,k),\\
V_2 &= \frac{1}{2(\beta^2-1)(k^2-\beta^2)}\{\beta^2E(u)+(k^2-\beta^2)u\\
&\quad +(2\beta^2k^2+2\beta^2-\beta^4-3k^2)\Pi(\phi,\beta^2,k)-\frac{\beta^4\,sn\,u\,cn\,u\,dn\,u}{1-\beta^2\,sn^2\,u}\},\\
\phi &= \sin^{-1}\sqrt{\frac{(\ell_2^2-\ell_4^2)(\ell^2-\ell_1^2)}{(\ell_1^2-\ell_4^2)(\ell^2-\ell_2^2)}},\quad sn\,u=\sin\phi,\\
\beta^2 &= \frac{\ell_1^2-\ell_4^2}{\ell_2^2-\ell_4^2},\quad \beta_1^2=\frac{\ell_2^2}{\ell_1^2}\beta^2,\\
k^2 &= \frac{\ell_2^2-\ell_3^2}{\ell_1^2-\ell_3^2}\beta^2,\quad g=\frac{2}{\sqrt{(\ell_1^2-\ell_3^2)(\ell_2^2-\ell_4^2)}}.
\end{aligned}$$

The solution is singular with respect to ε and does not smoothly continue to the collapse solution. At the point where ℓ^2 becomes minimum, that is,

$$\ell^2=\ell_1^2=\frac{C}{C-1}\frac{\varepsilon}{\kappa^2}=C\rho\eta, \tag{4.79}$$

ρ is equal to η, which is easily seen from eq.(4.73). This is the point where the partner of the boomerang journey is exchanged.

The boomerang interaction is shown in Fig.4.8(a) as well as the vortex collapse in (b). The boomerang interaction obtained by solving eq.(4.37) is depicted in Fig.4.9. Thus, for unshielded vortices, the divergence or explosion, gives unbounded vortex motion, which becomes bounded by the shielding effect. This is, after all, a result which was to be expected. We emphasize that three unshielded vortices can also

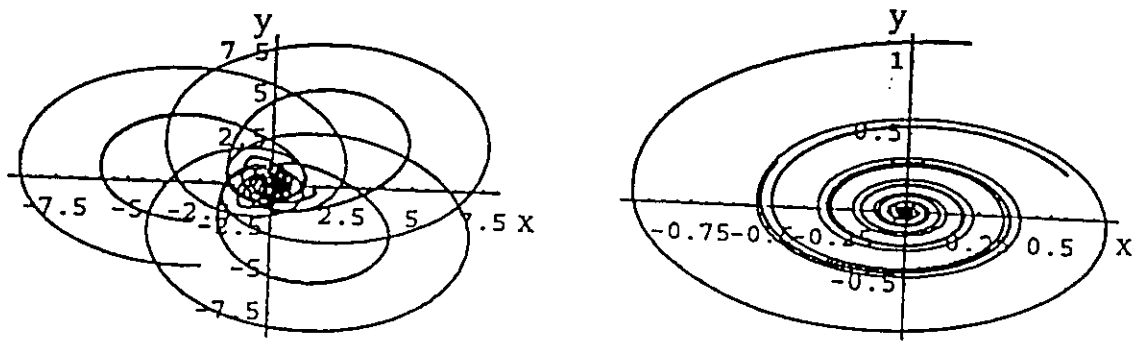

Figure 4.8: (a) the "boomerang interaction" of three vortices and (b) the vortex collapse

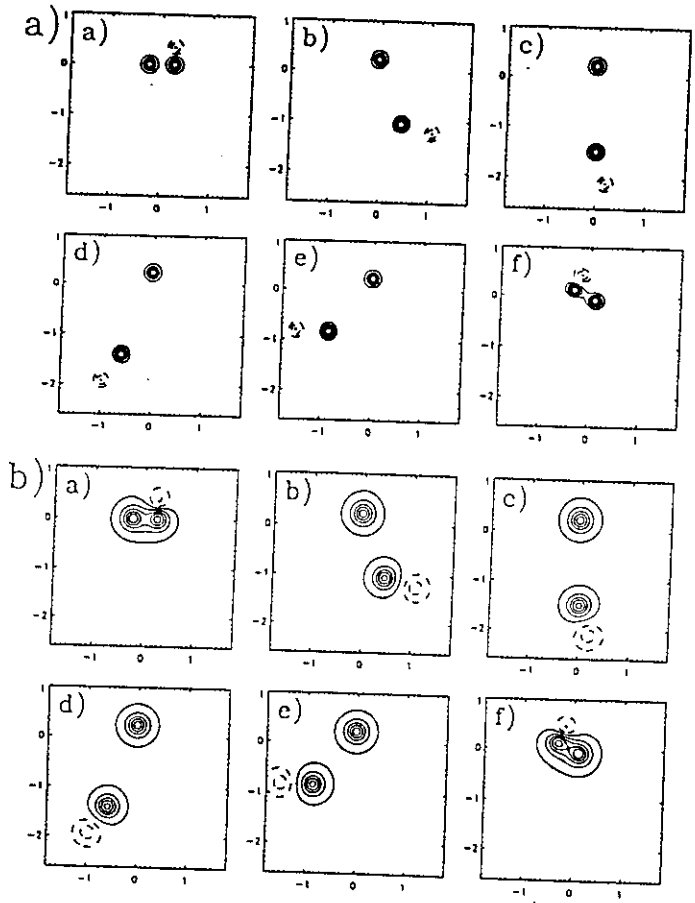

Figure 4.9: Numerical simulation of the "boomerang interaction".(a) potential and (b) vorticity

perform a bounded or localized motion, given a proper choice of vortices and initial positions, but these parameters will then not give a collapse by inversion. The vortex collapse is thought to provide a key to understanding of fundamental processes of strong turbulence. As discussed for instance by Novikov[11] and Novikov and Sedov[12], the collapse accounts for energy being systematically transferred into small scales, and for vortex dispersion, or "explosion", energy cascades into the large scales. The boomerang effect described here, an effect which owes its existence to the shielding effect ($\kappa \neq 0$), consequently corresponds to a "sloshing" of energy between large and small scales.

4.6 A statistical theory of point vortices and vortex diffusion

Here we turn to be a statistical system with N point vortices and derive an equation for vortex diffusion. Introducing a distribution function of vortices of j species by

$$F_\alpha(\mathrm{r},t) = \sum_j \delta(\mathrm{r} - \mathrm{r}_j^{(\alpha)}(t)), \tag{4.80}$$

we immediately obtain the Klimontovich equation [14] for vortices using eq.(4.37):

$$\frac{\partial}{\partial t} F_\alpha + \mathrm{z} \times \nabla\Phi \cdot \nabla F_\alpha = 0, \tag{4.81}$$

$$\Phi(\mathrm{r},t) = \frac{1}{2\pi} \sum_\alpha \int d\mathrm{r}'(\kappa_{\alpha 0} + v_* x') K_0(|\mathrm{r} - \mathrm{r}'|) F_\alpha(\mathrm{r}'). \tag{4.82}$$

The average distribution function is defined by the average over the ensemble of initial data:

$$< F_\alpha(\mathrm{r},t) >= \int d\mathrm{r}_{10} d\mathrm{r}_{20} \cdots d\mathrm{r}_{N0} P_\alpha(\mathrm{r}_{10}, \cdots, \mathrm{r}_{N0}) F_\alpha(\mathrm{r},t), \tag{4.83}$$

while the fluctuation part of the distribution function is simply given

$$\tilde{f}_\alpha(\mathrm{r},t) = F_\alpha(\mathrm{r},t) - < F_\alpha(\mathrm{r},t) >, \tag{4.84}$$

which includes fluctuations due to the interactions of the vortices and the dicreteness of the vortices. Taking the ensemble average of eq.(4.81), and subtracting the result from eq.(4.81), we obtain

$$\frac{\partial}{\partial t} < F_\alpha > + \mathrm{z} \times \nabla < \Phi > \cdot \nabla < F_\alpha >= - < \mathrm{z} \times \nabla\tilde{\Phi} \cdot \nabla \tilde{f}_\alpha >, \tag{4.85}$$

and

$$\frac{\partial}{\partial t} \tilde{f}_\alpha + \mathrm{z} \times \nabla(< \Phi > + \tilde{\Phi}) \cdot \nabla \tilde{f}_\alpha = -\mathrm{z} \times \nabla\tilde{\Phi} \cdot \nabla < F_\alpha > . \tag{4.86}$$

Introducing the Green's fuction

$$\{\frac{\partial}{\partial t} + \mathrm{z} \times \nabla(< \Phi > + \tilde{\Phi}) \cdot \nabla\} G(\mathrm{r},t|\mathrm{r}',t') = \delta(\mathrm{r} - \mathrm{r}')\delta(t - t'), \tag{4.87}$$

eq.(4.86) is formally solved in term of G by

$$\tilde{f}_\alpha(\mathrm{r},t) = \int d\mathrm{r}' dt' G(\mathrm{r},t|\mathrm{r}',t') \delta f(\mathrm{r}',t') - \int d\mathrm{r}' dt' G(\mathrm{r},t|\mathrm{r}',t') \mathrm{z} \times \nabla'\tilde{\Phi} \cdot \nabla' < F_\alpha >, \tag{4.88}$$

where δf is an initial condition. The Green's function is given by a solution of the characteristic equation of eq.(4.87) as

$$G(\mathbf{r},t|\mathbf{r}',t') = \delta(\mathbf{r}-\mathbf{r}(t;\mathbf{r}',t')), \tag{4.89}$$

where

$$\begin{aligned}\mathbf{r}(t;\mathbf{r}',t') &= \mathbf{r}' + \int_{t'}^{t} dt''\mathbf{z}\times\nabla[<\Phi(\mathbf{r}(t''),t'')> + \tilde{\Phi}(\mathbf{r}(t''),t'')] \\ &= \mathbf{r}' + \mathbf{U}_E(t-t') + \tilde{\mathbf{r}}(t;\mathbf{r}',t').\end{aligned} \tag{4.90}$$

Therefore the average Green's function is expected in terms of cumulants with respect to $\tilde{\mathbf{r}}$:

$$<G(\mathbf{r},t|\mathbf{r}',t')> = \sum_{\mathbf{k}} e^{i\mathbf{k}\cdot(\mathbf{r}-\mathbf{r}'-\mathbf{U}_E(t-t'))} e^{\sum_n C_n(\mathbf{k}\cdot\tilde{\mathbf{r}})}, \tag{4.91}$$

where $C_n(\mathbf{k}\cdot\tilde{\mathbf{r}})$ denotes the cumulants and the first two terms are given by

$$C_1(\mathbf{k}\cdot\tilde{\mathbf{r}}) = -i<\mathbf{k}\cdot\tilde{\mathbf{r}}>, \tag{4.92}$$

$$C_2(\mathbf{k}\cdot\tilde{\mathbf{r}}) = -\frac{1}{2}\{<(\mathbf{k}\cdot\tilde{\mathbf{r}})^2> - C_1(\mathbf{k}\cdot\tilde{\mathbf{r}})^2\} \tag{4.93}$$

Since our vortex system is characterized by complicated dynamical behavior of the constituent point vortices, the fluctuations are likely to deviate from the Gaussian, implying that the higher order cumulants do not vanish. However, we may assume, as a model, that the second order cumulant dominates over the others. Then eq.(4.91) is approximated by

$$<G(\mathbf{r},t|\mathbf{r}',t')> \simeq \sum_{\mathbf{k}} exp\{i\mathbf{k}\cdot[\mathbf{r}-\mathbf{r}'-\mathbf{U}_E(t-t')] - \mathbf{k}\cdot\mathbf{D}\cdot\mathbf{k}(t-t')\}, \tag{4.94}$$

where

$$\mathbf{D} = \frac{1}{2}\int_0^\infty d\mathbf{r} <\mathbf{z}\times\nabla\tilde{\Phi}(\mathbf{r}(t),t)\ \mathbf{z}\times\nabla\tilde{\Phi}(\mathbf{r}(t-t'),t-t')>, \tag{4.95}$$

and we have assumed that the correlation time of the fluctuations is short. Substituting eq.(4.88) into eq.(4.85), we have

$$\frac{\partial}{\partial t}<F_\alpha> + \mathbf{z}\times\nabla<\Phi>\cdot\nabla<F_\alpha> = \nabla\cdot\mathbf{D}\cdot\nabla<F_\alpha> + \mathbf{A}\cdot\nabla<F_\alpha>, \tag{4.96}$$

where

$$\mathbf{D} = \sum\int\frac{d\omega}{2\pi}\frac{\mathbf{z}\times\mathbf{k}:\mathbf{z}\times\mathbf{k}}{-i(\omega-\mathbf{k}\cdot\mathbf{U}_E)+\mathbf{k}\cdot\mathbf{D}\cdot\mathbf{k}}|\tilde{\Phi}(\mathbf{k},\omega)|^2, \tag{4.97}$$

$$\mathbf{A} = -\frac{i}{2\pi}\sum_{\mathbf{k}}\int\frac{d\omega}{2\pi}\frac{\mathbf{z}\times\mathbf{k}}{\varepsilon(\mathbf{k},\omega)}\frac{\kappa_0\hat{K}_0(\mathbf{k})+iv_*(\partial\hat{K}_0(\mathbf{k})/\partial k_x)}{(\omega-\mathbf{k}\cdot\mathbf{U}_E)^2+(\mathbf{k}\cdot\mathbf{D}\cdot\mathbf{k})^2}, \tag{4.98}$$

$$\varepsilon(\mathbf{k},\omega) = 1+\frac{i}{2\pi}\sum_{\mathbf{k}}\frac{\kappa_0\hat{K}_0(\mathbf{k})+iv_*(\partial\hat{K}_0/\partial k_x)}{-i(\omega-\mathbf{k}\cdot\mathbf{U}_E)+\mathbf{k}\cdot\mathbf{D}\cdot\mathbf{k}}\mathbf{k}\cdot\mathbf{z}\times\nabla<F_\alpha(\mathbf{r})>, \tag{4.99}$$

and $\hat{K}_0$ is the Fourier transform of $K_0(|\mathbf{r}|)$. The second term on the right-hand side of eq.(4.96) is a drag term due to the emission of wake fields by the vortices because of their discreteness:

$$<\delta f(\mathbf{r},t)\delta f(\mathbf{r}',t')> = F(\mathbf{r},t)\delta(\mathbf{r}-\mathbf{r}')\delta(t-t').$$

Since the characteristic frequency of the vortex fluctuation is simply the vortex turnover time, that is , $\omega \sim \mathbf{k} \cdot \mathbf{U}_E$ which is given by $\varepsilon(\mathbf{k}, \omega) = 0$, we may evaluate the vortex diffusion from eq.(4.97) as

$$D \sim \frac{1}{D} \sum_{\mathbf{k},\omega} |\tilde{\Phi}(\mathbf{k}, \omega)|^2 \sim \sqrt{\sum_{\mathbf{k},\omega} |\tilde{\Phi}(\mathbf{k}, \omega)|^2}, \tag{4.100}$$

which by eq.(4.82) with $\kappa_0 < v_* r_0$ approximately reduces to

$$D \sim N v_* r_0, \tag{4.101}$$

where r_0 is the average size of the vortices. The idea behind eq.(4.100) is illustrated in the following way. The quasilinear approximation for the vortex diffusion is to take into account the agitation of the orbit of a test vortex under the fluctuations induced by the other vortices that are assumed to be in a free motion, and it is given by

$$D \sim \sum \frac{k^2 |\tilde{\Phi}|^2}{\omega - \mathbf{k} \cdot \mathbf{U}_E}. \tag{4.102}$$

However, the vortices causing the fluctuations are themselves subject to diffusive motions. Therefore a self-consistent diffusion is given by replacing ω in the above expression by $\omega + ik^2 D$, leading to eq.(4.100).

From numerical experiments on the vortex collision, Horton found that the cross section σ for strong inelastic collisions is peaked at the impact parameter compatible to r_0 where $\sigma_{max} \simeq 2r_0$. Taking the average vortex speed as $c > v_*$, he estimated the vortex-vortex collision frequency as

$$\nu \sim n_v c \sigma \sim 2 n_v v_* r_0. \tag{4.103}$$

This leads to an effective diffusion D of the vortices

$$D \sim \nu r_0^2 \sim N v_* r_0, \tag{4.104}$$

which is the same result as that obtained in eq.(4.101) by the statistical theory for point vortices.

It is worthwhile to point out that the point vortex system introduced in this section may be subject to a phase transition to form a vortex lattice, since the interaction force between the point vortices is short range and a local order is likely to be formed. We suggest that further studies of the packing fraction $f_p = n_v \pi r_0^2$ and the vortex-vortex correlation function be used to distinguish between the turbulent states described as vortex gas [15], a vortex liquid and a density packed system approaching a vortex lattice.

References

[1] A. Hasegawa and K. Mima, Phys. Rev. Lett. 39, 205 (1977)

[2] J. Kono and T. Yamagata, Proc. Oceangr. Soc. Jpn. 36, 83 (1977)

[3] N. Zabusky and J. C. McWilliams, Phys. Fluids 25, 2175 (1982)

[4] W. Horton, Phys. Fluids **B1**, 524 (1989)

[5] A. Hasegawa, C. C. Maclennan and Y. Kodama, phys. Fluids **22**, 2122 (1979)

[6] M. Makino, T. Kamimura and T. Taniuti, J. Phys. Soc. Jpn **50**, 980 (1981)

[7] J. C. McWilliams and N. J. Zabusky, Geophys. Astrophys. Dyn. **19**, 207 (1982)

[8] J. Nycander and M. B. Isichenko, Phys. Fluids **B2**, 2042 (1990)

[9] M. Kono and E. Miyashita, Phys. Fluids **31**, 326 (1988)

[10] L. Onsager, Nuovo Cimento **6**, 279 (1949)

[11] E.A.Novikov, Sov. Phys. JETP **41**, 937 (1976)

[12] E.A.Novikov and Yu.B.Sedov, Sov. Phys. JETP **50**, 297 (1979)

[13] J. D. Meiss and W. Horton, Phys. Fluids **26**, 990 (1983)

[14] Yu. I. Klimontovich, *The Statistical Theory of Non-Equilibrium Processes in a Plasma* (MIT Press, Cambridge, MA, 1967)

[15] J. D. Meiss and W. Horton, Phys. Fluids **25**, 1838 (1982)

Chapter 5

Drift wave vortices in a cylindrical plasma

The Hasegawa-Mima equation [1] in a cylindrical plasma is written as

$$\frac{\partial \Pi}{\partial t} + [\psi, \Pi] + \mathbf{v}_* \cdot \nabla \psi = 0, \tag{5.1}$$

where ψ is an electrostatic potential and

$$\Pi = \psi - \nabla^2 \psi, \tag{5.2}$$

$$\mathbf{v}_* = \frac{v_T^2}{\Omega} \mathbf{z} \times \nabla_\perp \ln n_0. \tag{5.3}$$

When the background density is assumed to be a Gaussian, $n_0 \propto exp(-r^2/r_0^2)$, then the modulated point vortex model gives a set of equations as

$$\frac{d\mathbf{r}_\alpha}{dt} = -\frac{1}{2\pi} \sum_{\beta \neq \alpha} |\kappa_{\beta 0} - v_*(r_\beta^2 - \mathrm{r}_{\beta 0}^2)| \frac{\mathbf{z} \times (\mathbf{r}_\alpha - \mathbf{r}_\beta)}{|\mathbf{r}_\alpha - \mathbf{r}_\beta|} K_1(|\mathbf{r}_\alpha - \mathbf{r}_\beta|), \tag{5.4}$$

where $\kappa_{\beta 0}$ is the vorticity attached to the vortex β, v_* is given by $v_* = v_T^2/\Omega r_0^2$, and K_1 is the modified Bessel function of the second kind. Equation (5.4) has a constant of motion

$$P = \sum_\alpha |\kappa_\alpha - v_*(r_\alpha^2 - r_{\alpha 0}^2)|^2, \tag{5.5}$$

which is related to the fact that eq.(5.4) is invariant under the azimuthal rotation.

5.1 Dynamics of a vortex pair

For the system of two vortices, the relative distance of the vortices is a constant of motion in addition to the translational momentum.

$$r_{12}^2 = (x_1 - x_2)^2 + (y_1 - y_2)^2 = r_0^2 \tag{5.6}$$

with which eq.(5.4) is reduced to

$$\frac{dR}{dt} = -\frac{K_1(r_0)}{4\pi} f(R,\theta,\phi)\sin(\theta-\psi), \tag{5.7}$$

$$\frac{d\theta}{dt} = -\frac{K_1(r_0)}{2\pi r_0} g(R), \tag{5.8}$$

$$\frac{d\psi}{dt} = \frac{K_1(r_0)}{4\pi R} f(R,\theta,\psi)\cos(\theta-\psi), \tag{5.9}$$

where $x_1 - x_2 = r_0\cos\theta, y_1 - y_2 = r_0\sin\theta, (x_1+x_2)/2 = R\cos\psi, (y_1+y_2)/2 = R\sin\psi$, and

$$f(R,\theta,\psi) = \kappa_{10} - \kappa_{20} - 2v_* r_0[R\cos(\theta-\psi) - R_0\cos(\theta_0-\psi_0)], \tag{5.10}$$

$$g(R) = \kappa_{10} + \kappa_{20} - 2v_*(R^2 - R_0^2). \tag{5.11}$$

Here, R_0, θ_0 and ψ_0 are the initial values, repectively. Note that $f(R,\theta,\psi)$ and $g(R)$ satisfy the following condition:

$$f^2(R,\theta,\psi) + g^2(R) = 2P = 2(\kappa_{10}^2 + \kappa_{20}^2). \tag{5.12}$$

The dynamics of vortices is sensitive to their initial configuration and the magnitude of the value of v_*, κ_{10} and κ_{20} .

Introducing a new variable $\phi = \theta - \psi$, eqs.(5.7)-(5.9) reduce to

$$\frac{dR}{dt} = -\frac{K_1(r_0)}{4\pi} f(R,\phi)\sin\phi, \tag{5.13}$$

$$\frac{d\phi}{dt} = -\frac{K_1(r_0)}{2\pi r_0}[g(R) + \frac{r_0}{2R} f(R,\phi)\cos(\phi)]. \tag{5.14}$$

First, we consider the fixed points of the above equations, which are determined by

$$\sin\phi = 0, \quad g(R) + \frac{r_0}{2R} f(R,\phi)\cos\phi = 0. \tag{5.15}$$

The fixed points are given from eq.(5.15) for the case that $\kappa_{10} + \kappa_{20} \neq 0$ as

$$\phi = \phi_0 = n\pi, \quad R = R_0 = (-1)^{n+1}\frac{\kappa_{10} - \kappa_{20}}{\kappa_{10} + \kappa_{20}}\frac{r_0}{2} \tag{5.16}$$

These fixed points correspond to a vortex-pair moving on two concentric circles:

$$\theta = -[K_1(r_0)/\pi r_0(\kappa_{10} + \kappa_{20})]t, \quad and \quad \psi = \theta - n\pi.$$

The stability of these fixed points is examined by linearizing eqs.(5.13) and (5.14) around the fixed points, being given by

$$\frac{d}{dt}\delta R = -\frac{K_1(r_0)R_0}{2\pi r_0}(\kappa_{10} + \kappa_{20})\delta\psi, \tag{5.17}$$

$$\frac{d}{dt}\delta\phi = \frac{K_1(r_0)}{2\pi r_0 R_0}[\kappa_{10} + \kappa_{20} + v_*(4R_0^2 + r_0^2)]\delta R, \tag{5.18}$$

which shows that the fixed points are stable for $(\kappa_{10} + \kappa_{20})[\kappa_{10} + \kappa_{20} + v_*(4R_0^2 + r_0^2)] > 0$ and unstable otherwise. The unstable orbits are shown in Fig.5.1(b) -(f) and correspond to those of vortex-pairs in a slab geometry whose symmetry axis is initially tilted [2-3]. Special somtions are given for $\kappa_{10} = \kappa_{20}$ by

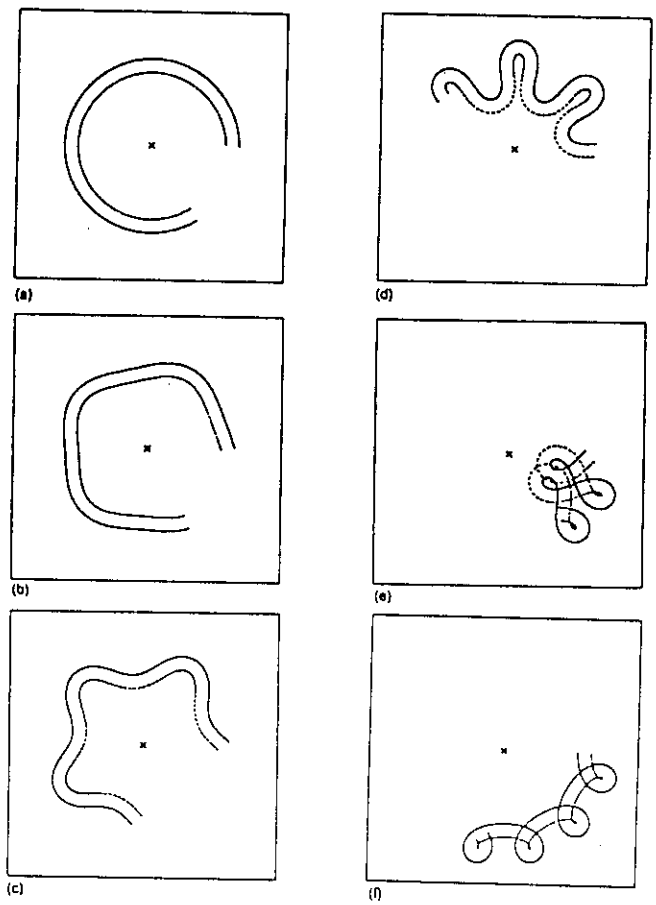

Figure 5.1: The motion of a vortex pair ($\kappa_1 = 11, \kappa_2 = -13$, and $r_* = 1$) corresponding to the observed for a slab plasma. The angle between the symmetry axis of the vortex-pair and the diamagnetic direction is (a) 0, (b) $\pi/12$, (c) $\pi/4$, (d) $\pi/2$, (e) $3\pi/4$, and (f) π.

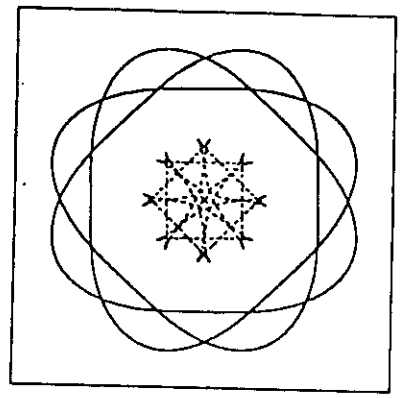

Figure 5.2: The periodic solution of a vortex-pair with $\kappa_1 = -\kappa_2 = 20$ and $v_* = 5$ for an initial condition $(x_1, y_1) = (3, 0)$ and $(x_2, y_2) = (-1, 0)$.

$$R = R_0 = 0, \tag{5.19}$$

$$\frac{d\phi}{dt} = -\frac{K_1(r_0)}{2\pi r_0}[2\kappa_{10} - v_* r_0^2(\cos\phi - \cos\phi_0)\cos\phi], \tag{5.20}$$

which is integrated for $\phi_0 = (n + 1/2)\pi$ to give

$$\tan\phi = \sqrt{\frac{2\kappa_{10} - v_* r_0^2}{2\kappa_{10}}}\tan(\sqrt{2\kappa_{10}(2\kappa_{10} - v_* r_0^2)}\frac{K_1(r_0)}{2\pi r_0}t + \frac{\pi}{2}). \tag{5.21}$$

For $2\kappa_0(2\kappa_0 - v_* r_0^2) < 0$, tan of the right hand side of eq.(5.21) is replaced by coth. In this case the two vortices rotate on the same circle.

When the following conditions hold, that is,

$$\kappa_{10} - \kappa_{20} + 2v_* r_0 R_0 \cos\phi_0 = 0, \tag{5.22}$$

$$v_*^2 r_0^4 + 2P - 2v_* r_0^2(\kappa_{10} + \kappa_{20} + 2v_* R_0^2) > 0, \tag{5.23}$$

periodic solutions are given by

$$g = \sqrt{2P}\frac{1 - Asn^2(\omega t, k)}{1 + Asn^2(\omega t, k)}, \quad A = \frac{\sqrt{2P} - g_2}{\sqrt{2P} + g2}, \tag{5.24}$$

where

$$\omega = \frac{K_1(r_0)}{4\pi r_0}\sqrt{(\sqrt{2P} - g_1)(\sqrt{2P} + g_2)}, \tag{5.25}$$

$$k = \sqrt{\frac{(1 - g_2)\sqrt{2P} + g_1}{(1 - g_1)\sqrt{2P} + g_2}}, \tag{5.26}$$

$$g_{1,2} = v_* r_0^2 \pm \sqrt{v_*^2 r_0^4 + 2P - 2v_* r_0^2(\kappa_{10} + \kappa_{20} + 2v_* R_0^2)}, \tag{5.27}$$

One of the periodic solutions is shown in Fig.5.2. When the condition does not hold, the solutions are quasiperiodic with two characteristic frequencies of rotations. One is associated with the motion around the center of mass and the other is around the axis of the cylinder.

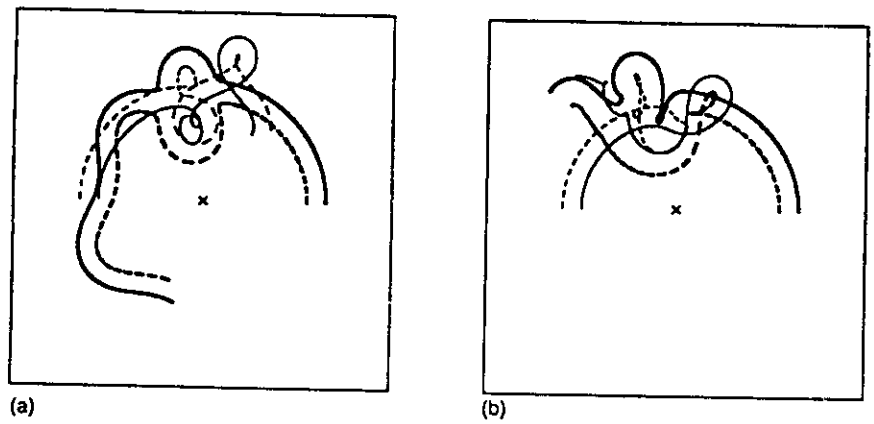

Figure 5.3: The head-on collision: (a) Zero impact parameter ($v_* = 1.0$), the vortices with $\kappa_1 = 11$ of the initial position $(x_1, y_1) = (3.25, 0)$ and $\kappa_2 = -15$ of the initial position $(x_2, y_2) = (-2.75, 0)$ are denoted by thick, solid and dotted lines, and those with $\kappa_3 = -11, (x_3, y_3) = (-3.25, 0)$ and $\kappa_4 = 13, (x_4, y_4) = (-2.75, 0)$ are by thin, solid, and dotted lines. (b) Nonzero impact parameter, the vortices with $\kappa_1 = 11$ of the initial position $(x_1, y_1) = (3.25, 0)$ and $\kappa_2 = -13$ of the initial position $(x_2, y_2) = (2.75, 0)$ are denoted by thick, solid and dotted lines, and those with $\kappa_3 = -10, (x_3, y_3) = (-3.0, 0)$ and $\kappa_4 = 12, (x_4, y_4) = (-2.5, 0)$ are by thin, solid, and dotted lines.

5.2 Collision processes of vortex-pairs

In a slab geometry head-on collisions and over-taking collisions are elastic for opposite-signed vortex-pairs with zero impact parameter, that is, the vortex-pairs preserve their identity through collision like soliton. This situation changes for a cylindrical plasma. Figure 5.3(a) shows the head-on collision of two vortex-pairs with zero impact parameter. After the collision they start to oscillate propagating in the azimuthal direction as if they started from tilted positions. Thus the collision as with zero impact parameter for a cylindrical plasma correspond to those with finite impact parameters for a slab plasma. Certainly, collisions with finite impact parameters for a cylindrical plasma are very much complicated performing as exchange scattering, trapping, and detrapping as is shown in Fig.5.3(b). In fact at the second round of the collision in Fig.5.3(a) the exchange scattering is observed. A common characteristic of collision process is a large radial excursion which may be a cause of anomalous cross field transport.

5.3 Dynamics in a bounded region

Introducing a complex variable $z = x + iy$, an equation for point vortex dynamics is generally rewritten as

$$\frac{dz_\alpha}{dt} = -\frac{\partial \Psi(z_\alpha)}{\partial z_\alpha}, \tag{5.28}$$

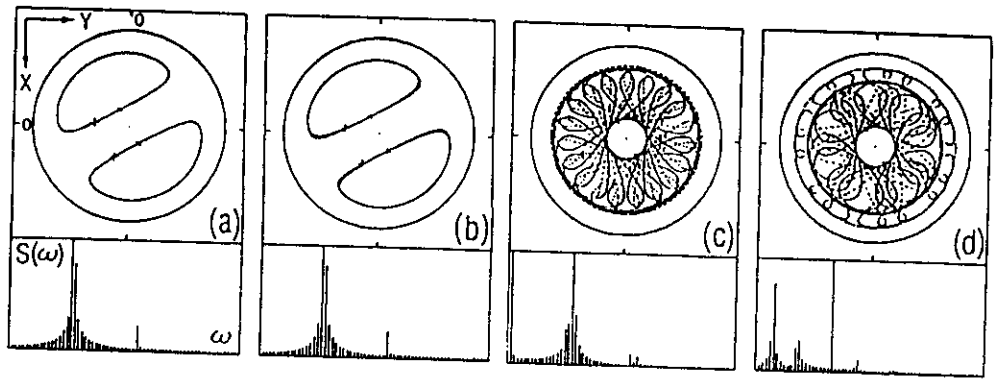

Figure 5.4: The trajectories of a vortex-pair ($\kappa_1 = -\kappa_2 = 4.0$) initially symmetric with respect to the origin $(x_1, y_1) = (-x_2, -y_2) = (3^{1/2}/10, 0.1)$: (a) $v_* = 0$, (b) $v_* = 0.005$, (c) $v_* = 0.5$, and (d) $v_* = 2.5$.

where Ψ is a complex potential and $\bar{z}$ is the complex conjugate of z. Now a boundary condition is readily included. When the plasma is confined in a conducting vessel of radius R, the effect of the wall is represented by mirror images of vortices in the vessel. According to the circle theorem [4] the potential $\Psi(z)$ is replaced by

$$w(z) = \Psi(z) + \bar{\Psi}\left(\frac{R^2}{z}\right). \tag{5.29}$$

Since the complex potential w is real on the circle $z = R^2/\bar{z}$, the stream function is zero on this circle, and the selected boundary condition is automatically satisfied. Then the equation in a cylindrical system is given by

$$\begin{aligned}\frac{dz_\alpha}{dt} &= -\frac{1}{2\pi i}\sum_{\beta\neq\alpha}(\kappa_\beta - v_*|z_\beta|^2)\frac{z_\alpha - z_\beta}{|z_\alpha - z_\beta|}K_1(|z_\alpha - z_\beta|) \\ &+ \frac{1}{2\pi i}\sum_{\beta\neq\alpha}(\kappa_\beta - v_*|\frac{R^2}{z_\beta}|^2)\frac{R^2}{z_\alpha^2}\frac{R^2/z_\alpha - \bar{z}_\beta}{|R^2/z_\alpha - z_\beta|}K_1(|R^2/z_\alpha - \bar{z}_\beta|),\end{aligned} \tag{5.30}$$

where we have assumed a Gaussian profile in a radial coordinate for the background density. The numerical solution is given in Fig.5.4 for different vales of v_*. The dynamical behavior becomes complicated when v_* is increased.

The dynamics for Euler's vortices in a bounded region has been intensively studied in [5-7].

References

[1] A. Hasegawa and K. Mima, Phys. Rev. Lett. 39, 205 (1977)

[2] N. Zabusky and J. C. McWilliams, Phys. Fluids 25, 2175 (1982)

[3] M. Makino, T. Kamimura and T. Taniuti, J. Phys. Soc. Jpn **50**, 980 (1981)

[4] L. M. Milne-Thomson, *Theoretical Hydrodynamics*(Macmillan, London, 1964), p154

[6] J. C. Hardin and J. P. Mason, Phys. Fluids **27**, 1583 (1984)

[7] Y. Kimura, Y. Kusumoto and H. Hashimoto, J. Phys. Soc. Jpn. **53**, 2988 (1984)

[8] Y. Kimmura and H. Hashimoto, J. Phys. Soc. Jpn. **55**, 5 (1986)